Journal of Thermal Analysis and Calorimetry (2023) 148:11435–11454
https://doi.org/10.1007/s10973-023-12458-w

Combustion, kinetics and thermodynamic characteristics of rice husks and rice husk-biocomposites using thermogravimetric analysis

Vianney Andrew Yiga[1,2] · Moses Katamba[2] · Michael Lubwama[2,3] · Karin H. Adolfsson[1] · Minna Hakkarainen[1] · Edwin Kamalha[4]

Received: 30 November 2022 / Accepted: 7 August 2023 / Published online: 8 September 2023

Abstract

Pyrolysis of rice husk (RH), alkali-treated cellulose-rich rice husk (RHC), chemically modified RHC (RHCM) and RH-biocomposites by thermogravimetric analysis was carried out to determine combustion and kinetic parameters at three different heating rates of 20, 40 and 50 °C min^{-1}. Combustion performance was analyzed from results of ignition temperature, burnout temperature, combustion rates, flammability index and combustion characteristic index. Increase in heating rate from 20 to 40 and further to 50 °C min^{-1} increased the onset of degradation, burnout and peak temperatures as observed by curve shifts to the right. Maximum combustion rates were around 0.57–0.59% min^{-1}, 1.03% min^{-1} and 0.63–0.69% min^{-1} for RH, RHC and RHCM, respectively. For the RH-biocomposites, the maximum combustion rates were in a 0.76–0.97% min^{-1} range. Their average pre-exponential factors using KAS method were in the 2.24E-03–8.07E-03 range, respectively, while those for OFW method were in the 7.75E + 04–4.55E + 06 range, respectively. Average activation energies of RH-biocomposites were in the 41.0–58.2 kJ mol^{-1} and 48.3–67.7 kJ mol^{-1} ranges for KAS and OFW methods, respectively. The data were well fitting with coefficient of determination (R^2) values close to 1. Average ΔG value ranges for RH-biocomposites ranged between 148.2 and 161.7 kJ mol^{-1}. The low-energy barrier ($\leq$5.4 kJ mol^{-1}) between activation energy and enthalpy changes indicated that reaction initiation occurs easily.

Keywords Alkali · Biocomposites · Combustion · Kinetics · Pyrolysis · Rice husks · TGA

Introduction

It has been reported that over 1.2 million tons of agricultural wastes was generated annually in Uganda [1]. One such agricultural waste material is rice husks [2, 3]. Rice (*Oryza sativa*) of lowland and upland species has become a staple food in Uganda, with an annual production growth rate of over 9% [4]. The processing of paddy into rice produces enormous amounts of husks (over 20% by mass) [5, 6]. In Uganda, the main disposal means for rice husks are open burning, a method that is associated with negative environmental effects [3, 7, 8]. Additionally, the burning practice of rice husks often leads to air pollution, and the airborne particles can cause respiratory diseases in humans [9]. The conversion of specific rice husks species into useful products like bioplastics or biocomposites could be facilitated by knowledge of their combustion characteristics, kinetics and thermodynamic behaviors [2]. This knowledge can guide the application of rice husk-derived materials to suitable fields as well as to suitable disposal methods [10]. Moreover, to study the influence of modification of rice husks, by e.g., alkali or acid, is important for production of biocomposites, because it modifies the chemical composition and makes their surfaces rougher, which improves adhesion with plasticizers and biopolymer matrices [11–13].

Combustion characteristics and kinetic behavior analysis is an important approach to study the mechanisms of the thermochemical conversion of a biomass material and the

✉ Vianney Andrew Yiga
yiga@kth.se; vianney.yiga@mak.ac.ug

1 Department of Fibre and Polymer Technology, KTH Royal Institute of Technology, SE-100 44 Stockholm, Sweden

2 Department of Mechanical Engineering, Makerere University, Kampala, Uganda

3 Africa Center of Excellence in Materials, Product Development and Nanotechnology, Makerere University, Kampala, Uganda

4 Department of Polymer, Textile and Industrial Engineering, Busitema University, Busia, Uganda

ICTAC Kinetic Committee recommended use of multiple heating rates to obtain more reliable combustion characteristic and kinetic parameters instead of single heating rates [14]. Combustion characteristics and kinetic parameters can be obtained by thermogravimetric analysis (TGA) [15–19]. Combustion characteristic parameters focus on combustion reaction mechanisms while kinetic parameters focus on activation energies of a given material [20]. Activation energy is the minimum amount of energy that reaction compounds need to hold in order to initiate a reaction. Various kinetics study on rice husks from different origins have been carried out using various methods [16, 21–25]. From these studies, it was observed that most works concentrated on obtaining activation energies, but only very few investigated rice husks' combustion and thermodynamic characteristics [22, 26]. A comparison of mean value of activation energy of rice husks utilized in the present study with those of rice husks from different origins is shown in Table 1. Table 1 illustrates that obtained activation energies vary depending on the kinetic/fitting method as well as heating rate utilized in their determination and that the obtained values are strongly variable depending on the hydrogeological differences in region or country. This further justifies the gap in determination of kinetic parameters of rice husks, especially for development of bioplastics because it is important for sustainability.

Although the body of research involving kinetics of rice husks from regions outside Uganda is sizable, it is still limited considering the large number of available species of rice husks. In fact, there exists differences in hydrogeological conditions from one region and country to another, which implies that physical properties of agricultural residues are expected to be geo-specific [33]. Additionally, weather conditions in a particular season greatly affect the quality of rice and accruing rice husks [34]. Moreover, there have been no attempts to determine the synergy of reaction combustion characteristics, kinetic and thermodynamic parameters of rice husks, and their different chemical modifications, aiming at production of biobased materials. Therefore, this research was aimed at characterizing K98 rice husk (RH) and products derived from the K98 RH, including two chemical modifications of rice husk and biocomposites with incorporated rice husk modifications. Especially, thermogravimetric analysis at different heating rates was utilized to determine their combustion, kinetic and thermodynamic

Table 1 Mean activation energies of rice husks from different origins

Rice husk origin	Heating rate/°C min^{-1}	Mean activation energy/kJ mol^{-1}	Fitting method	Reference
Indonesia	10, 20, 30, and 40	253.3	KAS	Kasmiarno et al. [16]
		251.6	OFW	
		33.9	Coats–Redfern	
India	5, 10, and 15	222.2–228.0	KAS	Kumar et al. [22]
		218.8–220.1	OFW	
		222.2–228.4	Starink	
India	2, 5, 10, 15, and 20	106.0 and 109.0	Coats–Redfern	Singh et al. [23]
		192.8 and 229.1	DAEM	
India	10, 20, and 30	72.3	KAS	Gajera et al. [27]
		73.1	OFW	
China	10	18.73–83.35	Coats–Redfern	Wang et al. [28]
China	20, 40, 60, 80, and 100	220.1	OFW	Jia et al. [21]
		224.9	Friedman	
		132.0	DAEM	
China	20	93.0–143.0	Coats–Redfern	Yuan et al. [24]
Egypt	10, 15, and 20	72.5–108.0	Direct Arrhenius	El-Sayed [29]
		124.5–175.5	Coats–Redfern	
		78.5–208.0	Sequential	
Malaysia	10, 20, 50, and 100	151.2–183.9	KAS	Loy et al. [30]
		153.6–185.7	OFW	
		152.6–190.8	Friedman	
Malaysia	10, 20, 30, and 50	48.6–54.2	KAS	Lim et al. [25]
China	10, 20, and 40	148.4	OFW	Zhang et al. [31]
		146.3	Starink	
China	5, 10, and 15	113.3–148.8	OFW	Gu et al. [32]

parameters. The kinetic parameters were obtained from TGA experimental data using Kissinger–Akahira–Sunose (KAS) and Ozawa–Flynn–Wall (OFW) methods.

Materials and methods

Materials

K98 Rice husk, from now called RH, with average particle size ≈0.85 mm was obtained from Tororo district in Eastern Uganda. K98 (*Supa*) is a fragrant, clean and sticky rice variety. Tororo district is located at latitude 0.45°, longitude 34.05° and approximately 208 km from Kampala city center. The RH had 13% moisture content. Sodium hydroxide (NaOH), potassium hydroxide (KOH), distilled water, isopropanol, sodium chlorite, hydrochloric acid, mono-chloroacetic acid and sulphuric acid (H_2SO_4) were supplied by Lab Access Uganda Ltd, Kampala, Uganda.

Processing

RH were washed with distilled water to remove any contaminants present in them. They were then oven-dried at 70 °C for 16 h. The dried RH were then crushed in a grinder and sieved through a 60-mesh screen before treatment with KOH alkali solution (6% w/v concentration and liquor ratio of 3:1) at 85 °C for 2 h [35–37]. This treatment is performed to remove some silica, lignin and hemicellulose. The obtained solid was filtered and washed using distilled water before new oven treatment at 70 °C for 16 h. Acid hydrolysis was then performed using sulphuric acid (4% v/v concentration), and the mixture was heat treated at 70 °C for 2 h. The aim of this treatment is to remove silica, amorphous parts of cellulose and remaining lignin and impurities. The obtained residue was again oven-dried at 70 °C overnight to recover a RH fraction rich in cellulose, abbreviated as RHC. The fraction was bleached by mixing with sodium chlorite (12% w/v) at 80 °C for 4 h before oven-drying at 70 °C overnight [35, 36]. Part of the RHC was modified through mercerization to increase its strength and for a lustrous appearance, by adding 100 mL of isopropanol and 20% w/v sodium hydroxide (NaOH) to 10 g of bleached RHC [35, 36, 38]. The mixture was stirred for 2 h at 60 °C, and the obtained residue was oven-dried at 70 °C for 4 h. The residue was then mixed with 100 mL of 20% w/v mono-chloroacetic acid and the solution and stirred for 4 h at 70 °C. The residue was washed with ethanol and HCl (37%) mixture at a 1:1 ratio to remove potassium ions, before oven-drying at 60 °C overnight to recover a RHC product, which was further chemically modified and abbreviated as RHCM.

Biocomposite film preparation

RHC-starch and RHCM-starch based biocomposites

1 g of RHC or RHCM was added to 40 mL of distilled water at 80 °C and stirred continuously. 1 g of gelatinized starch powder (for retrogradation) was then added in the solution and stirred to until homogenous solution was obtained [35, 36, 39]. This was followed by addition of first 7 g of glycerol plasticizer and then 4 g of acetic acid. The mixture was stirred for 40 min at 80 °C in a water bath until a precipitate was formed [40]. The precipitate was poured into a petri dish, spread to obtain the films, and left to cool at room temperature for 10 min before oven-drying at 55 °C for 16 h [41].

RHCM-gelatin-based biocomposites

1 g of RHCM was added to 40 mL of distilled water at 80 °C and stirred until the solution looked homogeneous. 1 g of gelatin powder (for gelatinization) was added, and the mixture was again stirred until it looked homogeneous. 7 g of glycerol plasticizer was added, and the mixture was stirred at 80 °C in a water bath for 40 min until a precipitate was formed [40]. The precipitate was poured into a petri dish, spread to obtain the films, and left to cool at room temperature for 10 min before oven-drying at 55 °C for 16 h [41].

Scanning electron microscopy (SEM) and energy-dispersive X-ray (EDX)

Morphology of RH, RHC, RHCM as well as developed RH-biocomposites was observed under a field emission scanning electron microscope (FESEM) coupled with energy-dispersive X-ray (EDX) spectroscopy, Carl Zeiss Sigma 300 VP model. Samples were attached on double-sided adhesive carbon tape, coated with a 0.2-nm chromium layer using a vacuum sputter coater (model Q 150 T ES), vacuum-dried and scanned at an acceleration voltage of 5.0 kV. EDX spectra were obtained at an acceleration voltage of 20.0 kV and collected for 19 s.

Thermogravimetric analysis (TGA)

Thermogravimetric analysis (TGA) (Eltra Thermostep non-isothermal Thermogravimetric analyzer, Haan, Germany) was used to determine mass loss of RH, RHC, RHCM as well as the developed RH-biocomposites as a function of temperature [19, 42, 43]. TGA was carried out according to the ASTM E1131 standard. The samples were heated from 40 to 600 °C at three different heating rates of 20, 40 and 50 °C min^{-1}. High-purity compressed air (Oxygen: Nitrogen = 21:79, > 99.99%) was used for cleaning the crucibles

and chamber prior to the TGA experiments. Nitrogen gas was used as the purge gas for pyrolysis experiments. The flow rate was maintained at 20 mL min^{-1} and the sample masses averaged 1.2 g. TGA also provided combustion explanations in terms of differential thermogravimetry (DTG), peak temperatures and mean reactivity of the RH, RHC, RHCM and the developed RH-derived biocomposites.

Combustion characteristic parameters

For each heating rate, ignition temperature, T_i is a measure of difficulty to ignite. A low ignition temperature suggests easy ignition, and vice versa. Burnout temperature, T_f refers to the temperature of the combustible substances in the completely burnt state. The ignition and burnout temperatures of RH, RHC, RHCM and the developed RH-derived biocomposites were determined according to the tangent method proposed by Liu et al. [44]. The flammability index, F, reflects the reactivity of the early stages of combustion and is expressed by Eq. (1).

$$F = \frac{\left(\frac{d\alpha}{dt}\right)_{max}}{T_i^2} \tag{1}$$

where $\left(\frac{d\alpha}{dt}\right)_{max}$ is the maximum combustion rate. The larger the value of flammability index, the more combustible a material is. The combustion characteristic index, S, reflects how quick the combustion rate is and is expressed by Eq. (2) [20].

$$S = \frac{\left(\frac{d\alpha}{dt}\right)_{max}\left(\frac{d\alpha}{dt}\right)_{mean}}{T_i^2 T_f} \tag{2}$$

where $\left(\frac{d\alpha}{dt}\right)_{mean}$ is the average combustion rate. The larger the combustion characteristic index, the better the combustion characteristics, and the more intense combustion is [45].

Kinetics modeling

From the Arrhenius equation ($k = Ae^{\left(\frac{-E}{RT}\right)}$), the rate constant in the kinetic equation is closely related to temperature. A is a pre-exponential factor and T is the absolute temperature. According to Xiao et al. [46], a non-isothermal process can be regarded as an isothermal process within an infinitesimal short time interval. As such, the kinetic equation for an isothermal homogeneous phase reaction can be adopted for the pyrolysis of RH, RHC, RHCM as well as developed RH-derived biocomposites under a programmed heating condition by the means of thermal analysis (see Eq. (3)).

$$\frac{d\alpha}{dt} = k \times f(\alpha) \tag{3}$$

where k is the rate constant of the reaction, α is the immediate mass loss ratio during pyrolysis and is given by Eq. (4), $f(\alpha)$ is a function that reflects the apparent kinetics of pyrolysis of substances, which is expressed as shown in Eq. (5).

$$\alpha = \frac{(m_0 - m)}{(m_0 - m_f)} \tag{4}$$

where m_0, m, m_0 are the initial, instantaneous and final masses of the sample, respectively.

$$f(\alpha) = (1 - \alpha)^n \tag{5}$$

where n is the order of the reaction.

Combining Eqs. (3)–(5), we obtain:

$$\frac{d\alpha}{dT} = \frac{A}{\beta} e^{\left(\frac{-E}{RT}\right)}(1 - \alpha)^n \tag{6}$$

For a given heating rate, $\beta = \frac{dT}{dt}$, Eq. (7) can be obtained as the non-isothermal reaction rate.

$$\frac{d\alpha}{dT} = \frac{d\alpha}{dt} \times \frac{dt}{dT} \tag{7}$$

Therefore, Substituting Eq. (6) into Eq. (7) gives:

$$\frac{d\alpha}{dT} = \frac{A}{\beta} e^{\left(\frac{-E}{RT}\right)}(1 - \alpha)^n \tag{8}$$

In current study, the data obtained from TGA/DTG were used to determine the kinetic parameters (activation energy (E) and pre-exponential factor (A)), based on Arrhenius equation. Further, these kinetic parameters can be estimated graphically by integrating Eq. (8) and then applying mathematical approximation for exponential term. Based on previous literatures, five different approximations were carried out and correspondingly, four iso-conversional (model free) models and a model fitting method were adopted to calculate the apparent activation energy (E) at specific conversion time (α) [17, 47]. Among the above five models, two integral forms namely Kissinger–Akahira–Sunose (KAS) model and Ozawa–Flynn–Wall (OFW) model were used in this study.

(a) Kissinger–Akahira–Sunose (KAS) method

In the KAS method, mathematical approximation for exponential term is assumed, and after approximation and rearrangement, the solution is given by Eq. (9) [48].

$$\ln\left(\frac{\beta_i}{T_{\alpha_i}^2}\right) = \ln\left(\frac{A_\alpha E_\alpha}{R.g(\alpha)}\right) - \frac{E_\alpha}{RT_{\alpha_i}} \quad (9)$$

A plot of $\ln\left(\frac{\beta_i}{T_{\alpha_i}^2}\right)$ against $\frac{-1}{T_{\alpha_i}}$ for a given value of conversion, α yields a straight line with slope $\frac{-E_\alpha}{R}$ and an intercept $\ln\left(\frac{A_\alpha E_\alpha}{R.g(\alpha)}\right)$, from which E_α can be calculated.

(b) Ozawa–Flynn–Wall (OFW) method

The OFW method uses the Doyle's approximation [49] and OFW equation is expressed by Eq. (10) [50].

$$\ln\beta_i = \ln\left(\frac{A_\alpha E_\alpha}{R.g(\alpha)}\right) - 5.332 - 1.052\frac{E_\alpha}{RT_{\alpha_i}} \quad (10)$$

where $g(\alpha)$ is constant at a given value of conversion. A plot of $\ln\beta_i$ against $\frac{1}{T_{\alpha_i}}$ for a given value of conversion, α yields a straight line with slope $\frac{-1.052E_\alpha}{R}$ and an intercept $\ln\left(\frac{A_\alpha E_\alpha}{R.g(\alpha)}\right) - 5.332$.

Thermodynamic analysis

The OFW method was used to obtain thermodynamic characteristics of RH, RHC, RHCM and the developed RH-derived biocomposites at a given heating rate, including change in Gibbs free energy (ΔG), change in enthalpy (ΔH) and change in entropy (ΔS) using Eqs. (11)–(13) [15, 51–54].

$$\Delta G = E_\alpha + \left(RT_m\right)\ln\left(\frac{K_B T_m}{hA}\right) \quad (11)$$

where $A = \frac{\beta E_\alpha e^{\left(\frac{E_\alpha}{RT_m}\right)}}{RT_m^2}$

$$\Delta H = E_\alpha - \left(RT_m\right) \quad (12)$$

$$\Delta S = \left(\frac{\Delta H - \Delta G}{T_m}\right) \quad (13)$$

where K_B is the Boltzmann constant, h is the Plank's constant, and T_m is the peak temperature during combustion.

Results and discussion

Surface morphology

Surface morphology of K98 RH at different magnifications is shown in Fig. 1a–c. The rice husk appeared irregular in shape with a size varying in micron order. They formed a well-organized, rigged and compact block-like structure with dented lumps and straight ridges [55–57]. These structures are formed by cementing non-cellulosic materials complexed with cellulose [58]. The structures were punctuated with prominent domes [59, 60].

Figure 1d–i shows the surface morphology of RHC and RHCM produced by chemical modification, respectively. Cellulose fibers typically have long, small cavity and irregular fibrous structure with various thickness [61]. Rice husks fiber bundles are separated into individual fibers in plant cells, as lignin and hemicellulose are deposited between the cellulosic micro-fibrils forming an interrupted lamellar structure [62]. Chemical modifications to form RHC and RHCM were found to alter the surface structure of remaining larger RHC and RHCM particles, by revealing a more dominant fibrillary network on the outer surface [55, 63]. Surfaces were rougher after the modification because the chemical treatment is expected to remove particulated material (lignin, hemicellulose, fats and waxes) from the surface of the rice husks [11, 64]. Fiber bundles were also released, individualized and visualized as microfibrils. This result agrees with those reported Johar and Ahmad [65] and Nascimento et al. [66].

Figure 2a–c shows the surface morphology of RHC-starch biocomposites indicating relatively good adhesion between RHC and starch matrix although some voids in the interfacial boundary were observed in some locations. These voids will act as sites of stress concentration and as a load is applied, fracture at these sites is expected to occur. These regions (see Fig. 2a, b) therefore present some amount of areas with poor bonding between RHC and starch. This result is similar to those obtained by Yap [67] and Bisht et al. [68].

Surface morphologies seen in Fig. 2d–f for RHCM-starch biocomposites showed both large-sized voids and various small-sized voids, and also the surface appears to have more roughness and topological variation (see Fig. 2d) [69]. Figure 2g–i presents surface morphologies for RHCM-gelatin-based biocomposite. This material appears to have the most homogeneous dispersion of RHCM compared to the other biocomposites. This can be attributed to the potentially more favorable interactions such as H-bonding interaction between RHCM and gelatin matrix [70]. Most of the fibers were firmly attached to the matrix without voids. A smoother surface (see Fig. 2i) also indicates improved adhesion between RHCM and gelatin matrix as result of surface modification through introduction of carboxyl groups, which may favorably interact with amine groups in gelatin. Similar observations were obtained by Bisht et al. [68] and Marichelvan et al. [71].

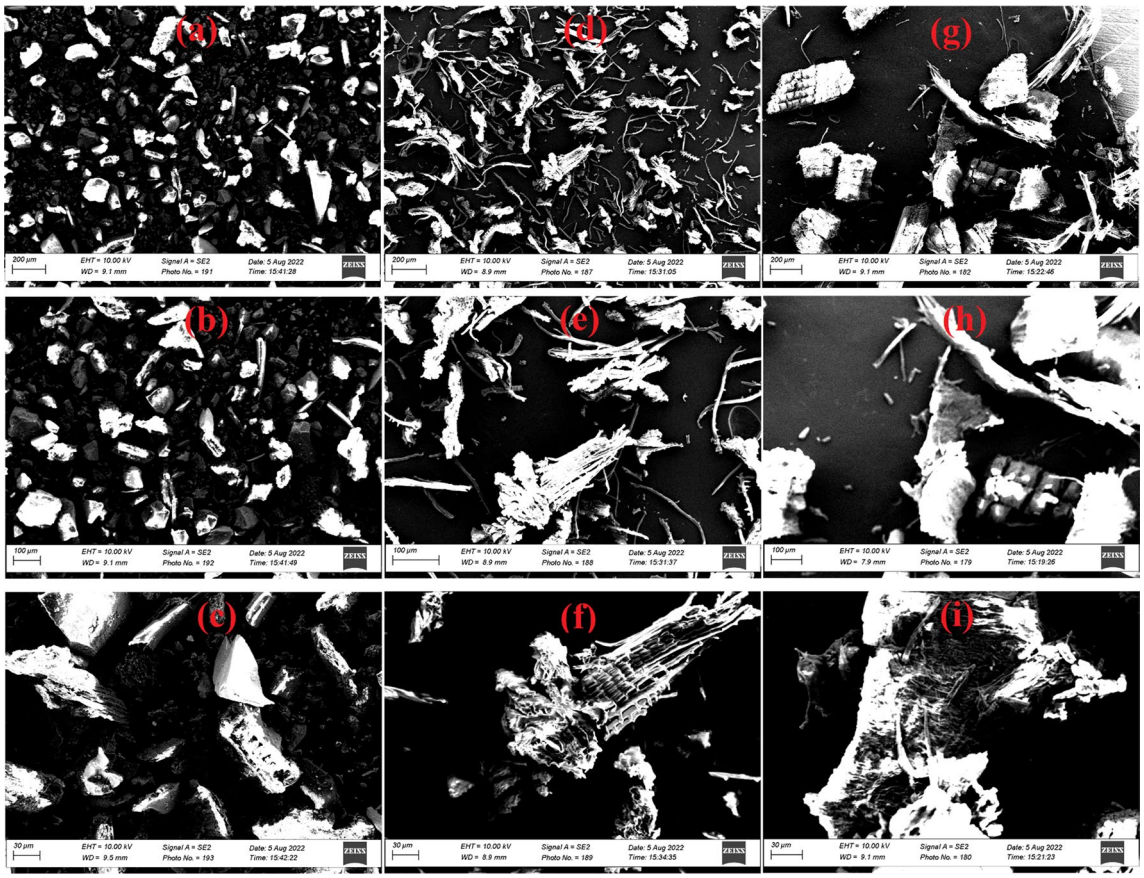

Fig. 1 Surface morphologies for **a**, **b**, **c** K98 RH; **d**, **e**, **f** RHC; **g**, **h**, **i** RHCM at different magnifications

Elemental analysis of surfaces by EDX

Elemental analysis by EDX revealed that the RH, RHC, RHCM and biocomposite samples had carbon and oxygen as the main constituents with other elements such as silicon, aluminum and sodium having very small percentages (see Fig. 3). As expected there was a high carbon–oxygen ratio (2.1:1) in the K98 RH. The carbon–oxygen ratio for RHC and RHCM were reduced to 1.1:1 and 1:1.1, respectively (see Table 2). The decreased carbon–oxygen ratio supports removal of lignin, which should have higher carbon–oxygen ratio compared to cellulose. These findings are similar to those obtained by Onoja [72] and could be explained by removal of more carbon-rich lignin from the materials. Na increased because of some entrapped Na^+ from alkali treatment. The samples had very small silica peaks, especially for the developed RH-derived biocomposites. The silica content in RH, RHC and RHCM was as expected higher compared to the RH-derived biocomposites (see Fig. 3d–f). It should be noted that to form RHC, alkali treatment did not significantly reduce the amount of silica, but in RHCM, the amount was greatly reduced. From EDX also, only trace amounts of Mg, Al, and K were detected with no significant changes due to alkali treatment.

Thermal analysis by TG and DTG

Figure 4 presents the TGA curves of RH, RHC and RHCM (Fig. 4a–c) as well as accruing RH-derived biocomposites (Fig. 4d–f) at three different heating rates of 20, 40 and 50 °C min^{-1}. The curves show the typical appearance of pyrolysis of RH and from them, the thermal phases for each of the heating rates can be located [23, 73]. It is evident that the complete pyrolysis process for all the samples can be divided into three major stages. The first stage from 40 to 300 °C causes degradation and hence mass loss ($\leq 8\%$) of some light components, including inbound water and light volatile components [16, 17, 23, 30, 69, 74, 75].

The second stage between 300 and 425 °C causes the maximum mass loss (40–50%) during thermal degradation. From the percentage loss in mass, it is clear that the degradation rate of the developed rice husk-derived biocomposites (see Fig. 4d–f) was higher compared to the RH, RHC and RHCM (see Fig. 4a–c) at the same temperature range under consideration. Moreover, for

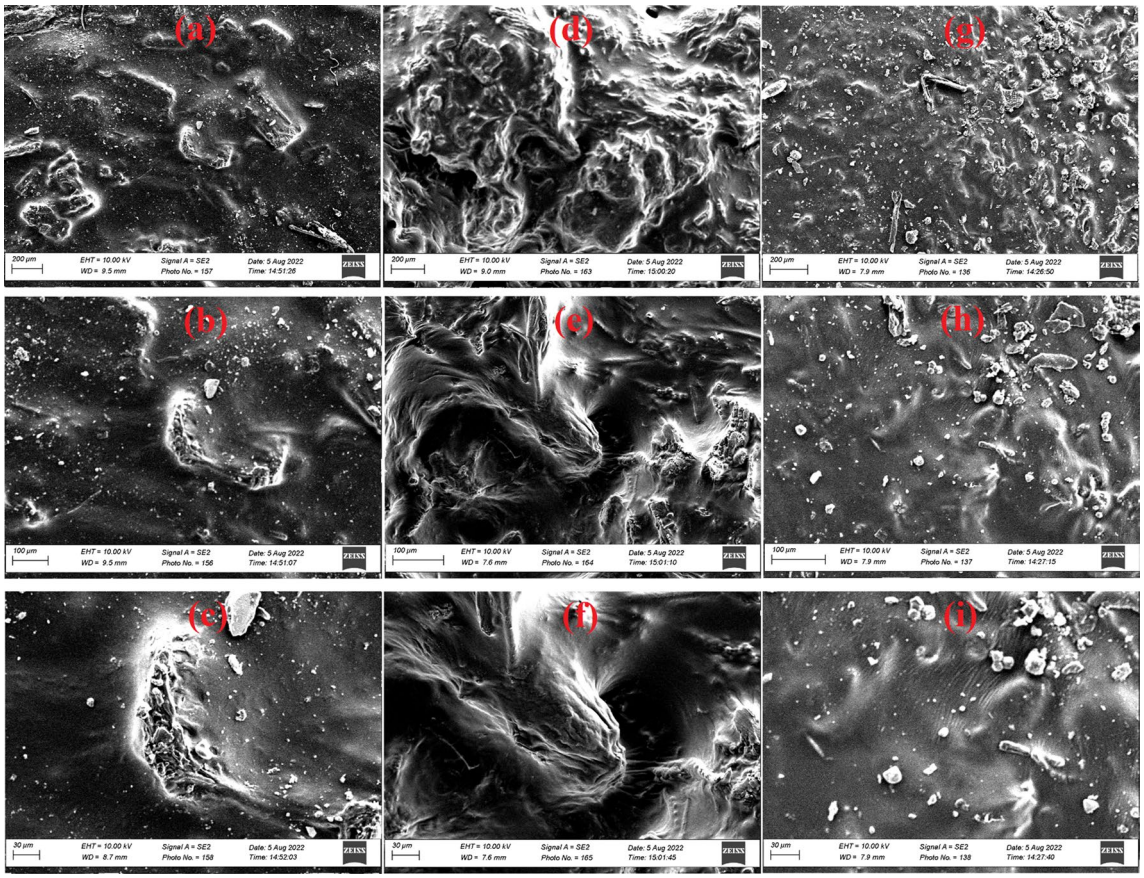

Fig. 2 Surface morphologies for RH-derived biocomposites **a**, **b**, **c** RHC-starch; **d**, **e**, **f** RHCM-starch; **g**, **h**, **i** RHCM-gelatin at different magnifications

RH-derived biocomposites, the major mass loss in this range was possibly due to the decomposition of gelatin and starch [71]. An increase in heating rate leads to a clear shift of this phase to the right-hand side, signaling that higher temperatures are required to cause decomposition of hemicellulose and cellulose [76]. At lower heating rate, sufficient time is available for more heating, achieving linear temperature profile between the outer surface and inner

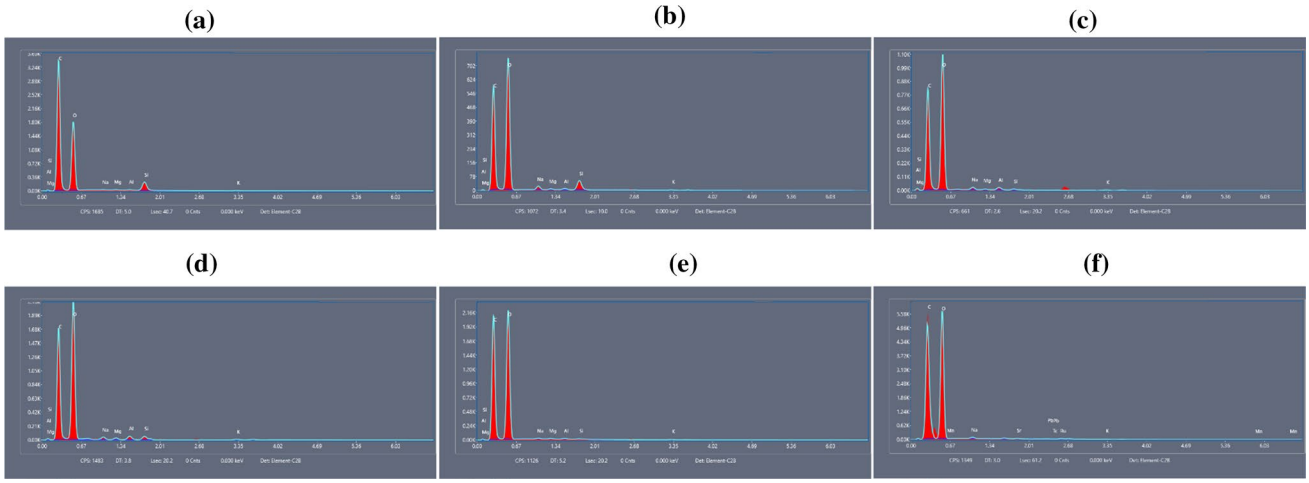

Fig. 3 EDX spectra for **a** K98 RH; **b** RHC; **c** RHCM; **d** RHC-starch biocomposite; **e** RHCM-starch biocomposite; **f** RHCM-gelatin biocomposite

Table 2 Elemental compositions for EDX of K98 RH, RHC, RHCM and RH-derived biocomposites

Element	Mass/%					
	K98 RH	RHC	RHCM	RHC-starch	RHCM-starch	RHCM-gelatin
C	65.7	50.1	48.0	51.7	53.8	49.3
O	32.0	46.4	50.2	47.1	45.3	49.3
Na	0.05	0.89	0.64	0.19	0.22	0.31
Si	2.0	2.04	0.21	0.44	0.11	–

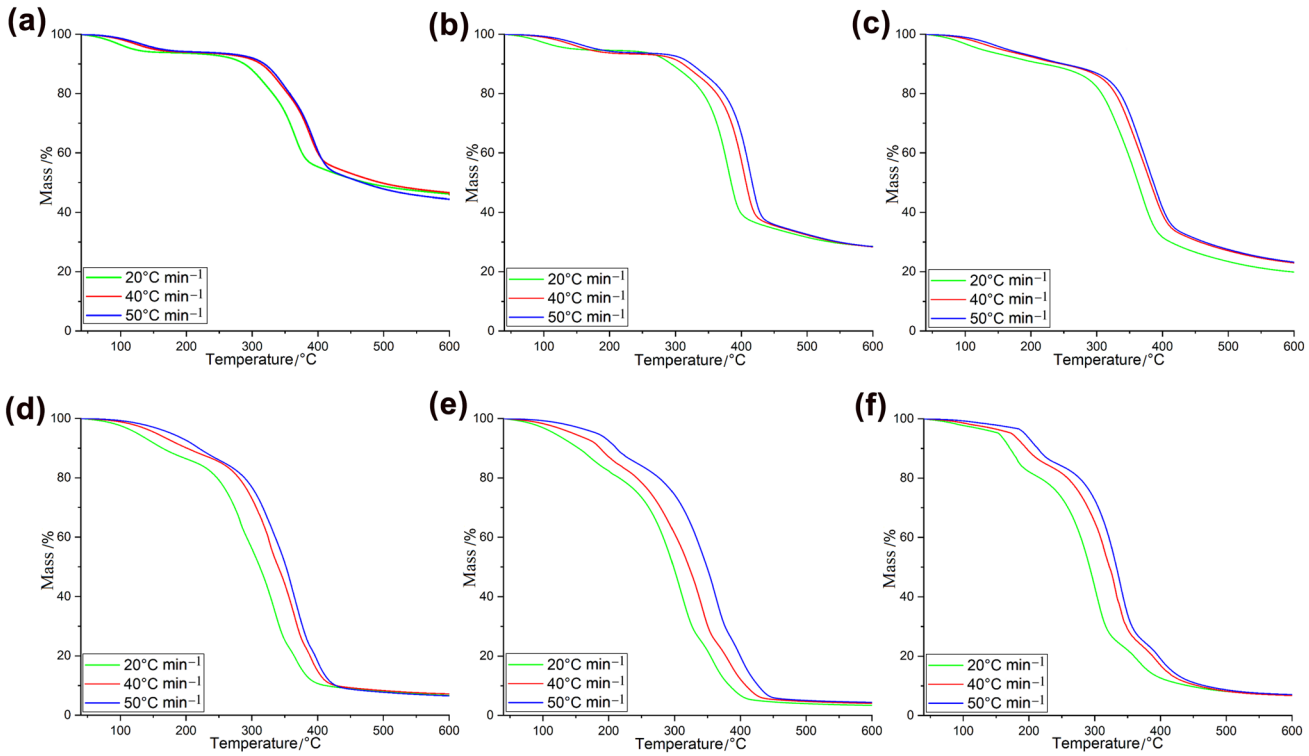

Fig. 4 TG curves for **a** K98 RH; **b** RHC; **c** RHCM; **d** RHC-starch biocomposite; **e** RHCM-starch biocomposite; **f** RHCM-gelatin biocomposite

core of the RH, while at the higher heating rate, there is shorter exposure time and possible temperature gradient between outer and inner core of the RH [22, 77].

In the third stage, from 425 to 600 °C, any remaining lignin in the RH is decomposed and the mass loss continues until char residues are left at the maximum decomposition temperature [69, 78]. The char residues left were in ranges 44.4–46.1%, 28.4–28.5% and 19.9–30.3% for RH, RHC and RHCM, respectively. For RHC-starch, RHCM-starch and RHCM-gelatin, the ranges for char residues were 6.5–7.2%, 3.4–4.4% and 6.8–7.1%, respectively. The lower residues are deduced to the lower contents of inorganics and lignin in the biocomposites. The presence of these compounds can also promote the carbonization of polysaccharides leading to high char yields (see Table 2).

Figure 5 presents the differential thermogravimetric (DTG) curves of RH, RHC and RHCM (Fig. 5a–c) as well as accruing RH-derived biocomposites (Fig. 5d–f) at three different heating rates of 20, 40 and 50 °C min^{-1}. The rate of mass loss (% min^{-1}) is very low during the first stage, whereas it is higher in the second stage of the decomposition process, where hemicellulose and cellulose are expected to be decomposed from the rice husks [20, 79, 80].

The second stage of degradation shows the peak temperature ranges at 3364.8–393.5 °C, 380.3–413.3 °C and 365.1–380.8 °C for RH, RHC and RHCM, respectively. These high peak temperatures are important in application, especially during processing of RH-biocomposite packaging, so that they are able to withstand processing temperatures before severe degradation. In confirmation, peak temperature ranges for RHC-starch, RHCM-starch and RHCM-gelatin biocomposites were 334.9–365.6 °C, 310.4–362.3 °C and 301.1–337.4 °C, respectively. These

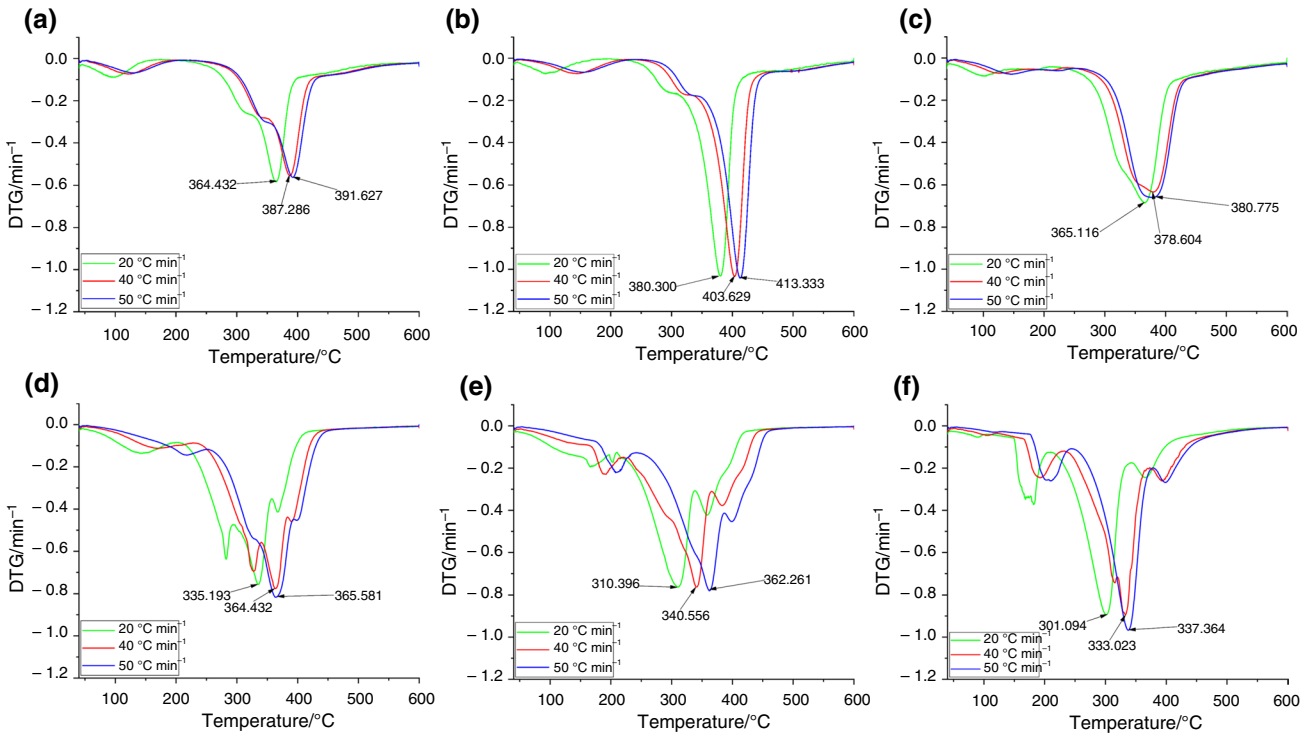

Fig. 5 DTG curves for **a** K98 RH; **b** RHC; **c** RHCM; **d** RHC-starch; **e** RHCM-starch; **f** RHCM-gelatin

temperatures are above thermal stability ranges reported in previous studies [71, 74, 81]. It should be noted that increase in heating rate leads to increasing peak temperatures as observed by the shifts of the peaks to the right, due to shorter exposure time at higher heating rates, so the temperature where degradation is initiated will be higher [16, 30, 53, 82, 83]. For example, for RHCM-gelatin, increase in heating rate from 20 to 40 °C min^{-1} led to increasing peak temperatures from 301.1 to 333.0 °C. Further increase in heating rate to 50 °C min^{-1} increased the peak temperature to 337.4 °C (see Fig. 5f).

Combustion characteristics parameters

The combustion characteristic parameters of the RH, RHC, RHCM as well as accruing RH- derived biocomposites are shown in Table 3. Increase in heating rate led to an increase in ignition, peak and burnout temperatures. This result confirms the results for thermal stability presented in Figs. 4 and 5. For example, increasing heating rate from 20 to 40 °C min^{-1} led to increase in ignition temperature from 290.6 to 309.3 °C for RH. Further increase in heating rate to 50 °C min^{-1} increased ignition temperature further to 326.7 °C. This trend is consistent with the results obtained by El-Sayed and Mostafa [18]. In a similar trend, increasing heating rate from 20 to 40 °C min^{-1} led to increase in ignition temperature from 226.3 to 258.8 °C for RHC-starch biocomposite. Further increase in heating rate to 50 °C min^{-1} increased ignition temperature to 269.6 °C. Increasing ignition and burnout temperatures signal enhanced thermal stability since higher temperatures are required to onset degradation of the RH, RHC and RHCM [84]. This result is again desired for packaging materials to provide wide processing window. Similar results were shown by El-Sayed [29] who reported that increase in heating rate of rice husks from 10 to 15 °C min^{-1} led to increase in ignition temperature from 258.0–262.0 to 258.0–264.0 °C, respectively. Maximum combustion rates of raw rice husks were around 0.57–0.59% min^{-1}, 1.03% min^{-1} and 0.63–0.69% min^{-1} for RH, RHC and RHCM, respectively. RH-biocomposites' maximum combustion rates were at a 0.76–0.97% min^{-1} range. These low values signal high flame retardancy due to reducing flammability and combustion characteristic indices [85]. A similar trend was observed for average combustion rates. For these, RH, RHC and RHCM had equal rates of 0.10% min^{-1}, 0.13% min^{-1} and 0.14% min^{-1}, respectively, while the developed RH-biocomposites reached higher rates of 0.17% min^{-1}.

Table 3 Combustion characteristics parameters for K98 RH, RHC, RHCM and RH-biocomposites

Sample	Heating rate	Temperature/°C			Combustion rate/% min^{-1}		Flammability index(10^{-5})	Combustion characteristic index (10^{-8})	Mean reactivity(10^{-3})
	°C min^{-1}	Ignition	Peak	Burnout	Maximum	Average	% min^{-1} °C^{-2}	% min^{-2} °C^{-3}	% min^{-1} °C^{-1}
K98 RH	20	290.6	364.8	407.5	0.59	0.10	0.69	0.16	1.61
	40	309.3	388.3	433.3	0.57	0.10	0.60	0.13	1.47
	50	326.7	393.5	433.3	0.58	0.10	0.55	0.13	1.48
RHC	20	329.1	380.3	408.7	1.03	0.13	0.95	0.30	2.71
	40	352.2	403.6	432.0	1.03	0.13	0.83	0.25	2.55
	50	361.5	413.3	440.9	1.04	0.13	0.80	0.23	2.52
RHCM	20	279.5	365.1	412.4	0.69	0.14	0.88	0.30	1.89
	40	298.9	378.6	426.6	0.63	0.14	0.71	0.23	1.66
	50	304.0	380.8	431.0	0.66	0.14	0.71	0.23	1.73
RHC-starch	20	226.3	334.9	382.5	0.76	0.17	1.48	0.66	2.27
	40	258.8	364.4	408.7	0.78	0.17	1.16	0.48	2.14
	50	269.6	365.6	417.3	0.82	0.17	1.13	0.46	2.24
RHCM-starch	20	220.5	310.4	368.2	0.76	0.17	1.56	0.72	2.45
	40	244.9	340.6	391.8	0.76	0.17	1.27	0.55	2.23
	50	271.1	362.3	417.1	0.78	0.17	1.06	0.43	2.15
RHCM-gelatin	20	226.5	301.1	346.9	0.89	0.17	1.73	0.85	2.96
	40	256.8	333.0	377.2	0.89	0.17	1.35	0.61	2.67
	50	272.2	337.4	383.9	0.97	0.17	1.31	0.58	2.87

Flammability index and combustion characteristic index values were minimal. For example, maximum flammability index and combustion characteristic index were 1.73×10^{-5}% min^{-1} °C^{-2} and 0.85 × 10–8% min^{-2} °C^{-3} for RH-biocomposites, respectively. The values generally decreased with increase in heating rate. This was expected since it takes longer to transfer heat from the external environment to the interior of the samples, thereby creating a hysteresis effect [20]. Moreover, the low flammability and combustion characteristic indices obtained indicate that the samples generally have very poor combustion performance [86, 87]. Low flammability and combustion characteristic are desired for biocomposites, not least in packaging applications so that there is no conduction heat transfer between the packaged material and the packaging material. It was, however, clear that RHC and RHCM are more combustible than the original non-modified RH, since their flammability and combustion characteristic indices are higher [45]. This is expected because during alkali modification to form RHC and RHCM, some thermally stable compounds like silica and lignin are erased from the surface of the rice husks [88]. RH, RHC and RHCM had mean reactivities in the range of 1.48×10^{-3}–2.71×10^{-3}% min^{-1} °C^{-1}, while the produced biocomposites had reactivities around 2.14×10^{-3}–2.96×10^{-3}% min^{-1} °C^{-1}. Low mean reactivity is desired so that the RH, RHC and RHCM burn with less ability, thereby enhancing the flame retardancy of produced biocomposites [55].

Kinetics analysis

The variation in degree of conversion of RH, RHC and RHCM (Fig. 6a–c) as well as accruing RH-biocomposites (Fig. 6d–f) as a function of temperature at different heating rates of 20, 40 and 50 °C min^{-1} are shown in Fig. 6. In order to compute the kinetic parameters, the same values of conversion rate (α) in the range of 0.2–0.8 were considered for the three heating rates [15, 17]. This range was considered because during the fitting of data using the KAS and OFW methods, the lowest conversion value (0.1) and the highest conversion value (0.9) did not fit well because of lower correlation values [51, 89]. As the temperature rises, conversion rates increased due to reduction in original mass of the RH (see Eq. (4)). The trend followed by the conversion curves is similar to that presented in TG and DTG curves, which present a decomposition in original mass (see Figs. 4 and 5). Moreover, increase in heating rate tends to shift the conversion curve to the right, signaling higher temperatures are required to decompose constituents of RH, RHC, RHCM and RH-biocomposites at higher heating rates. Similar depictions have been presented elsewhere [52, 53, 76].

Kinetic parameters of RH, RHC and RHCM and RH-biocomposites, such as activation energy and pre-exponential factor for pyrolysis, were determined using KAS and OFW methods based on the thermogravimetric analysis data obtained under different heating rates, based on the

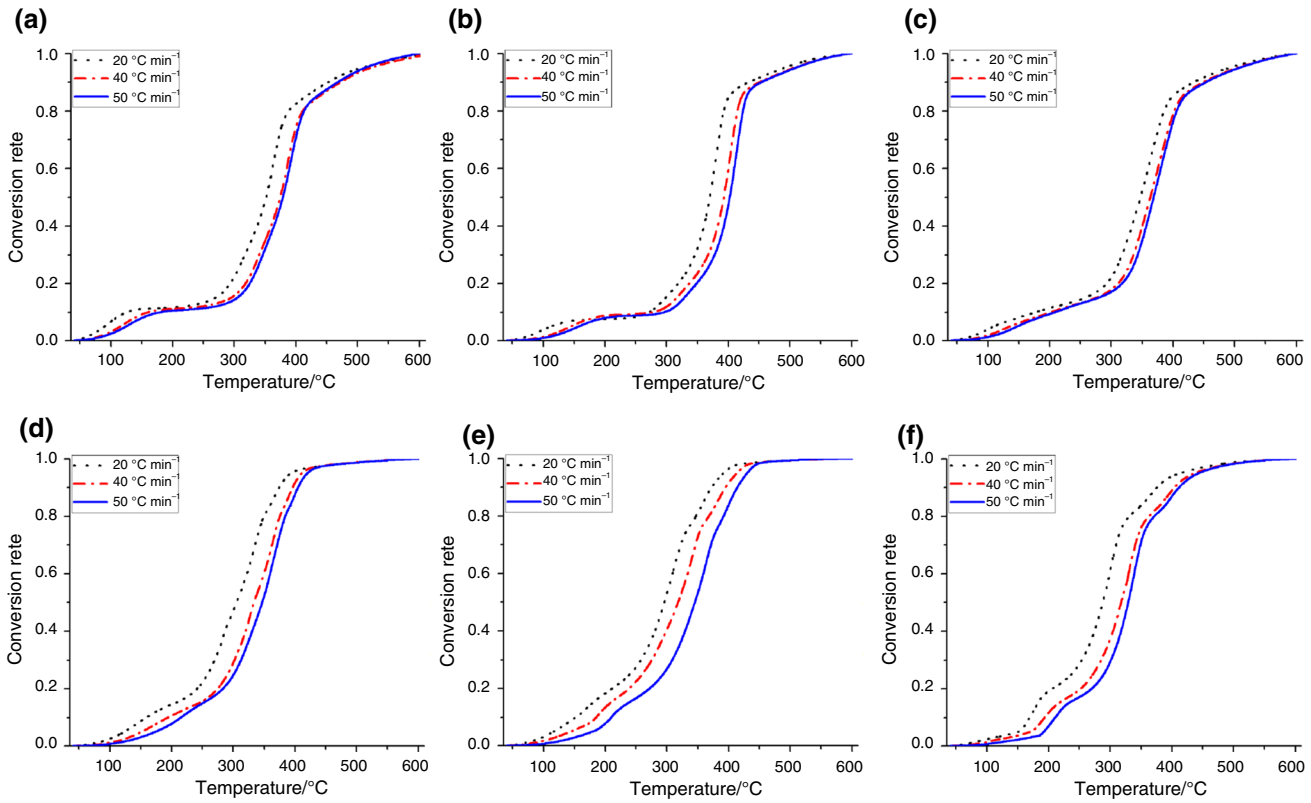

Fig. 6 Conversion curves for **a** K98 RH; **b** RHC; **c** RHCM; **d** RHC-starch; **e** RHCM-starch; **f** RHCM-gelatin

thermogravimetric analysis data obtained under different heating rates [15]. According to Liu et al. [20], activation energy is the energy required to transform molecules from normality to an active state in which reaction can easily occur. Using the KAS method, activation energies for progressive conversion values need to be calculated according to Eq. (9). Figure 7 shows the KAS linear plots of ln (β/T^2) versus 1/T for the conversion values within 0.2–0.8 for RH, RHC, RHCM (Fig. 7a–c) and RH-biocomposites (Fig. 7d–f). The calculated activation energies and pre-exponential factors from the slopes and intercepts of the KAS plots are listed in Table 4.

Using the OFW method, activation energies for progressive conversion values need to be calculated according to Eq. (10). Figure 8 shows the OFW linear plots of ln (β) versus 1/T for the conversion values within 0.2–0.8 for RH, RHC and RHCM (Fig. 7a–c) as well as accruing RH-biocomposites (Fig. 7d–f). The calculated activation energies and pre-exponential factors from the slopes and intercepts of the OFW plots are listed in Table 4.

The apparent activation energies, corresponding pre-exponential factors as well as respective R^2 values that were obtained from the slopes in each method are shown in Table 4. For RH, RHC, RHCM and accruing RH-biocomposites, R^2 values were close to 1, signaling accuracy and reasonability of the fitting method for the values of the three heating rates [76, 90]. Similar results were reported by Yuan et al. [91] who found that all the correlation coefficients away from straight line were > 0.95, which indicated the reliability of kinetic parameters evaluated by linear fitting. Both activation energy and pre-exponential factors generally increased with increase in conversion rate because as temperatures increased, changes in mass of the sample became minimal and therefore more energy was required for a reaction or for transformation to occur. Moreover, high pre-exponential factors depict low frequency of molecular collisions in the reaction mixture [52]. Additionally, the range for the obtained pre-exponential factors for each method had quite narrow ranges, which indicated the reliability of computed activation energy values [53].

Average activation energy of RH, RHC and RHCM was 95.9 kJ mol^{-1}, 94.0 kJ mol^{-1} and 123.4 kJ mol^{-1}, respectively, using the KAS method. The respective activation energies using the OFW method were 101.2 kJ mol^{-1}, 99.7 kJ mol^{-1} and 127.1 kJ mol^{-1}. These high activation energies are attractive for material to be used as packaging [20]. In fact, for RHC-starch, RHCM-starch and RHCM-gelatin, activation energies were 58.2 kJ mol^{-1}, 41.0 kJ mol^{-1} and 49.5 kJ mol^{-1} or 67.7 kJ mol^{-1}, 48.3 kJ mol^{-1} and 56.1 kJ mol^{-1} for KAS and OFW methods, respectively.

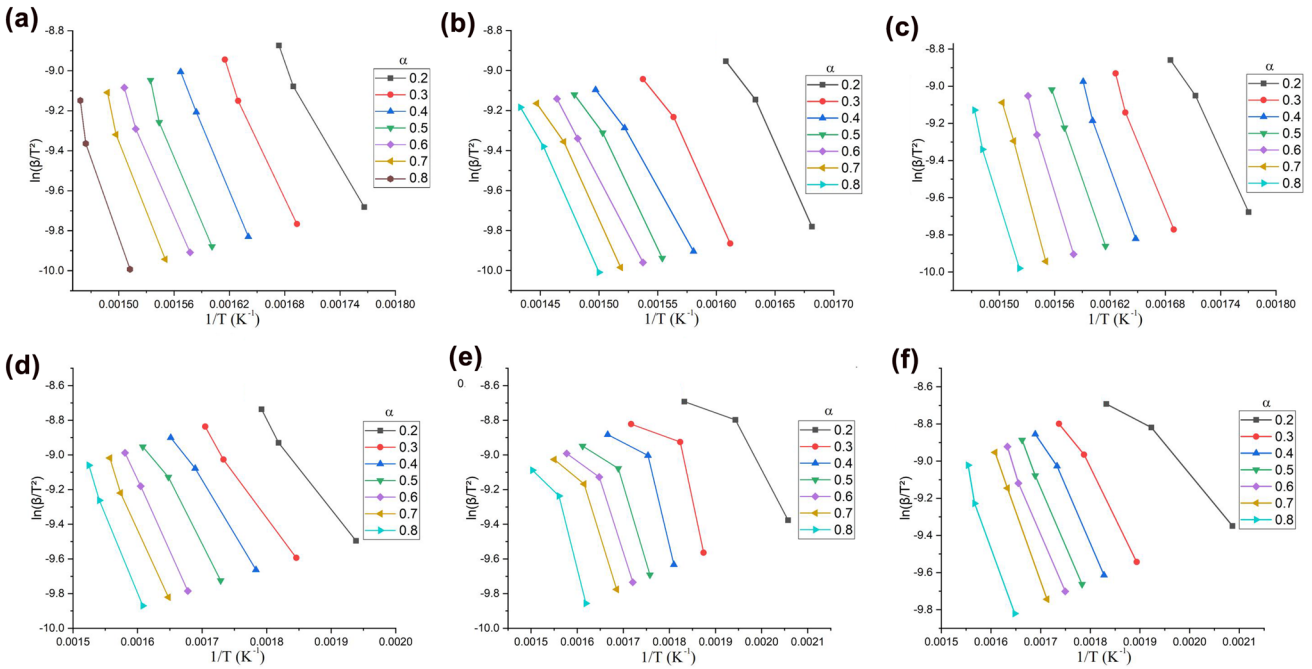

Fig. 7 Kinetic plots for **a** K98 RH; **b** RHC; **c** RHCM; **d** RHC-starch; **e** RHCM-starch; **f** RHCM-gelatin by KAS method

Average pre-exponential factors using KAS method for RH, RHC and RHCM were in the 0.24E + 00–1.10E + 03 range, respectively, while those for OFW method were in the 1.57E + 08–7.04E + 11 range, respectively. For developed RH-biocomposites, average pre-exponential factors using KAS method were in the 2.24E-03–8.07E-03 range, respectively, while those for OFW method were in the 7.75E + 04–4.55E + 06 range, respectively. From this, it was clear that the reaction during KAS was slower than that during OFW [52].

The variation of activation energy with increase in conversion rate (α) is shown in Fig. 9, depicting that the activation energy of RH, RHC and RHCM (Fig. 9a–c) as well as accruing RH-biocomposites (Fig. 9d–f) is highly dependent on the conversion rate. This also confirmed the complexity of the process of RH, RHC, RHCM pyrolysis, since their pyrolysis reaction is not a one-step reaction [17, 20, 26, 92]. The low correlation coefficient (R^2) of conversion rate values less than 0.2 and greater than 0.8 is not considered. From Fig. 9, it is clear that increase in conversion rate led to increasing activation energy, due to thermal degradation of different components of RH, RHC, RHCM and RH-biocomposites with increasing temperature. This trend is similar to other studies based on rice husks [23]. The weaker bonds (lower molecular mass compounds) decayed at moderate energy and lesser temperatures, while degradation of stronger bonds (higher molecular mass compounds) needed more energy at greater temperature [20]. It should be noted that OFW method presented higher activation energy values compared to the KAS method, but the variations among these methods at each conversion rate were minimal. This was consistent with other literature such as rice husks [30], hazelnut husks [93] and sawdust as well as rice husks [94]. Lower activation energies for RH-biocomposites could be due to chemical reaction which washed away some thermally stable compounds form the surfaces of the rice husks [95].

Thermodynamic parameters

Thermodynamic parameters of RH, RHC, RHCM and RH-biocomposites at three heating rates of 20, 40 and 50 °C min^{-1} were calculated using the OFW method, as shown in Eqs. (11)–(13) and are presented in Table 5. It is clear that pre-exponential factors and ΔH (enthalpy of reaction) increased with increase in heating rate, while Gibb's free energy (ΔG) showed an opposite trend as increasing heating rates led to a decrease in the ΔG value. The ΔH (enthalpy of reaction) is the energy exchanged between reactants and products during the chemical reaction [53]. The low-energy barrier ($\leq$5.4 kJ mol^{-1}) between the activation energies (see Fig. 9) and the ΔH values for the process indicated that reaction initiation can occur easily, due to the fact that the lower difference between ΔH and activation energy favors the complex formation [30, 32, 53, 54]. This result agrees well with works of Loy et al. [30] on rice husks pyrolysis as well as works of Rasool et al. [94] on rice husks and saw dust pyrolysis. Average ΔH value ranges (depending on heating rate) of RH, RHC and RHCM were 95.6–95.9 kJ mol^{-1},

Table 4 Kinetic parameters for K98 RH, RHC, RHCM and RH-biocomposites

Sample	Conversion rate (α)	Activation energy/ kJ mol^{-1}		Pre-exponential factor/ min^{-1}		R^2	
		KAS	OFW	KAS	OFW	KAS	OFW
K98 RH	0.2	71.20	76.80	5.9E-03	2.8E+06	0.9987	0.9990
	0.3	84.30	89.70	5.8E-02	3.0E+07	0.9956	0.9964
	0.4	95.30	100.50	3.5E-01	2.0E+08	0.9938	0.9949
	0.5	98.50	103.70	5.2E-01	3.1E+08	0.9880	0.9901
	0.6	101.30	106.50	8.0E-01	4.9E+08	0.9902	0.9919
	0.7	103.80	109.00	1.2E+00	7.5E+08	0.9900	0.9918
	0.8	117.00	121.80	9.1E+00	6.0E+09	0.9705	0.9753
	Average	95.90	101.20	1.7E+00	1.1E+09	0.9895	0.9913
RHC	0.2	95.83	100.69	2.92E-01	1.57E+08	0.9856	0.9883
	0.3	94.02	99.40	1.38E-01	8.05E+07	0.9829	0.9863
	0.4	81.72	87.95	1.46E-02	8.76E+06	0.9958	0.9968
	0.5	92.68	98.51	1.02E-01	6.34E+07	0.9907	0.9927
	0.6	92.78	98.72	1.10E-01	7.00E+07	1.0000	1.0000
	0.7	97.20	103.04	2.47E-01	1.62E+08	0.9907	0.9926
	0.8	104.02	109.65	8.25E-01	5.55E+08	0.9964	0.9972
	Average	94.037	99.71	0.246926	1.57E+08	0.9917	0.9934
RHCM	0.2	81.84	86.93	5.34E-02	2.57E+07	0.9911	0.993
	0.3	107.15	111.38	4.47E+00	2.39E+09	0.9928	0.9939
	0.4	120.72	124.13	4.33E+01	2.45E+10	0.9947	0.9955
	0.5	120.05	124.08	3.37E+01	1.98E+10	0.9999	0.9999
	0.6	140.90	144.08	1.15E+03	7.11E+11	0.9974	0.9977
	0.7	151.25	154.12	5.67E+03	3.64E+12	0.9996	0.9996
	0.8	141.66	145.20	7.94E+02	5.27E+11	0.9948	0.9955
	Average	123.37	127.13	1099.80	7.04E+11	0.9958	0.9964
RHC-starch	0.2	41.93	48.32	5.82E-05	2.21E+04	0.9941	0.9958
	0.3	43.80	50.52	7.68E-05	3.22E+04	0.9972	0.9980
	0.4	48.68	55.46	1.91E-04	8.69E+04	0.9967	0.9979
	0.5	54.35	61.13	5.22E-04	2.55E+05	0.9875	0.9913
	0.6	68.21	74.52	5.99E-03	3.15E+06	0.9999	1.0000
	0.7	71.62	77.93	1.10E-02	6.02E+06	0.9952	0.9963
	0.8	79.13	85.30	3.86E-02	2.23E+07	0.9966	0.9973
	Average	58.24	64.74	0.008067	4.55E+06	0.9953	0.9967
RHCM-starch	0.2	25.38	32.26	1.50E-03	1.14E+03	0.8686	0.9241
	0.3	34.42	41.55	4.40E-04	6.66E+03	0.6839	0.7787
	0.4	40.79	47.88	1.94E-04	2.42E+04	0.7727	0.8396
	0.5	41.69	49.02	3.03E-04	2.90E+04	0.8527	0.8998
	0.6	43.18	50.64	3.63E-04	4.12E+04	0.8877	0.9244
	0.7	46.46	53.94	2.87E-04	8.15E+04	0.9004	0.932
	0.8	55.27	62.67	6.47E-04	3.59E+05	0.8922	0.9226
	Average	41.03	48.28	0.000533	77,481.06	0.8369	0.8887
RHCM-gelatin	0.2	22.17	29.13	3.60E-03	5.90E+02	0.9690	0.9847
	0.3	40.43	47.13	1.01E-04	2.12E+04	0.9883	0.9925
	0.4	46.53	53.20	1.71E-04	7.38E+04	0.9904	0.9936
	0.5	52.97	59.51	5.93E-04	2.71E+05	0.9991	0.9993
	0.6	54.38	61.03	7.96E-04	3.78E+05	0.9957	0.9968
	0.7	62.74	69.15	3.84E-03	1.93E+06	1.0000	1.0000
	0.8	67.26	73.80	6.61E-03	3.59E+06	0.9854	0.9889
	Average	49.50	56.13	0.002244	8.94E+05	0.9897	0.9937

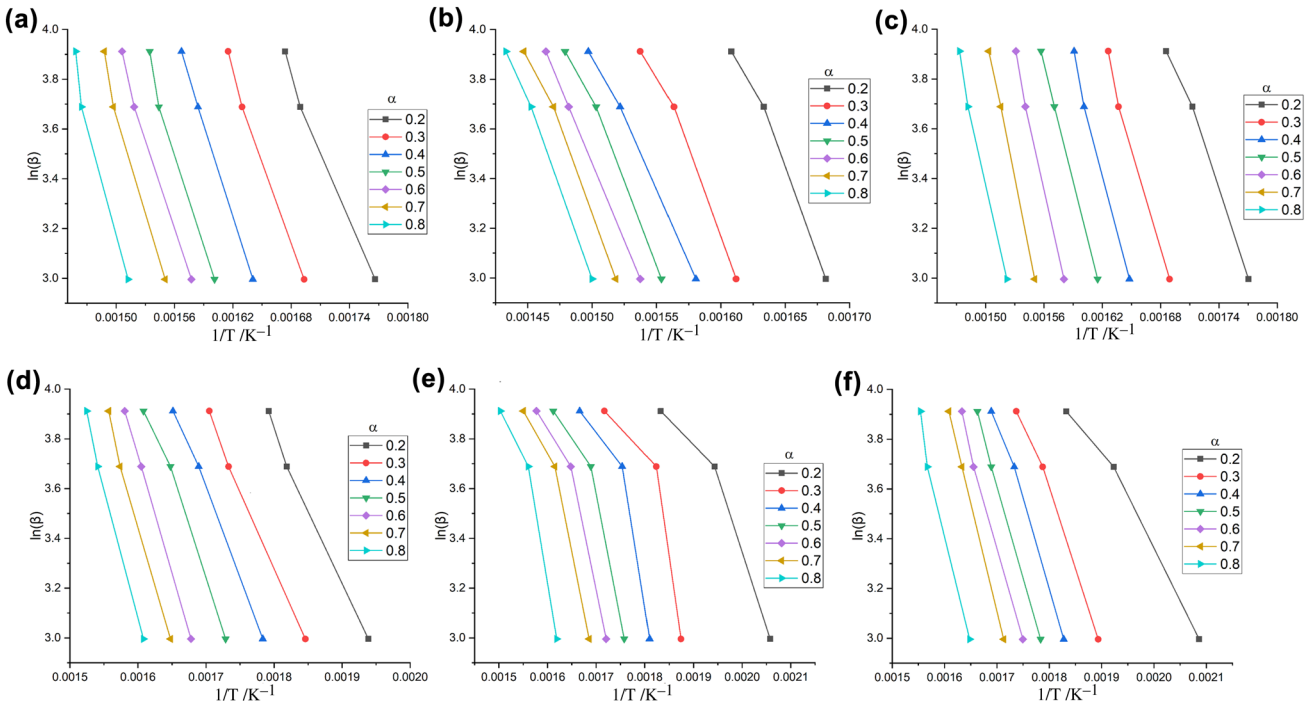

Fig. 8 Kinetic plots for **a** K98 RH; **b** RHC; **c** RHCM; **d** RHC-starch; **e** RHCM-starch; **f** RHCM-gelatin by OFW method

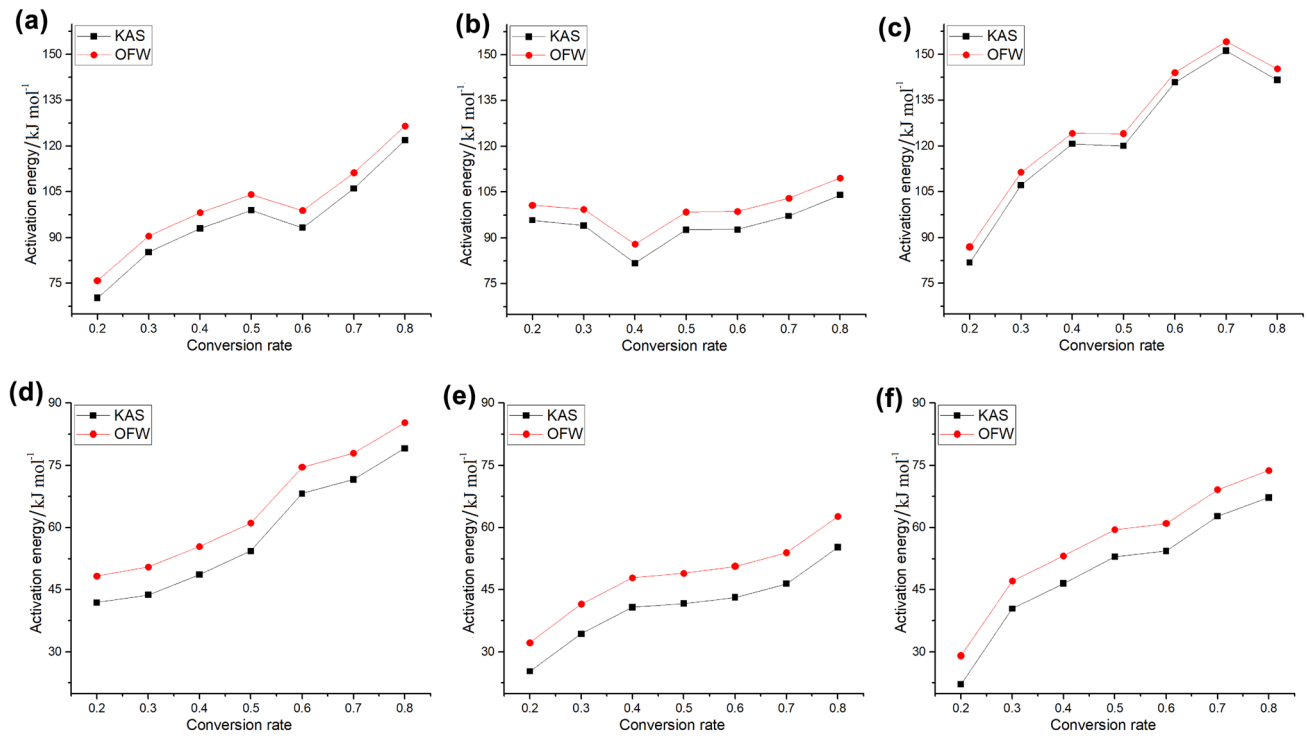

Fig. 9 Activation energy versus conversion rates for **a** K98 RH; **b** RHC; **c** RHCM; **d** RHC-starch; **e** RHCM-starch; **f** RHCM-gelatin

Table 5 Thermodynamic parameters for K98 RH, RHC, RHCM and RH-derived biocomposites

Sample	α	A/min^{-1}			ΔH/kJ mol^{-1}			ΔG/kJ mol^{-1}			ΔS/kJ mol^{-1} K^{-1}		
		20 °C min^{-1}	40 °C min^{-1}	50 °C min^{-1}	20 °C min^{-1}	40 °C min^{-1}	50 °C min^{-1}	20 °C min^{-1}	40 °C min^{-1}	50 °C min^{-1}	20 °C min^{-1}	40 °C min^{-1}	50 °C min^{-1}
K98 RH	0.2	8.9E+05	9.9E+05	1.1E+06	71.5	71.3	71.3	164.4	167.3	167.5	−0.15	−0.15	−0.14
	0.3	1.2E+07	1.2E+07	1.3E+07	84.4	84.2	84.2	163.6	166.4	166.6	−0.12	−0.12	−0.12
	0.4	1.0E+08	9.6E+07	1.0E+08	95.2	95.0	94.9	163.0	165.8	166.0	−0.11	−0.11	−0.11
	0.5	1.9E+08	1.8E+08	1.9E+08	98.4	98.2	98.2	162.8	165.6	165.8	−0.10	−0.10	−0.10
	0.6	3.3E+08	3.0E+08	3.2E+08	101.2	101.0	101.0	162.7	165.5	165.7	−0.10	−0.10	−0.10
	0.7	5.5E+08	4.9E+08	5.2E+08	103.7	103.5	103.5	162.6	165.3	165.5	−0.09	−0.09	−0.09
	0.8	6.8E+09	5.6E+09	5.8E+09	116.5	116.3	116.3	162.0	164.7	164.9	−0.07	−0.07	−0.07
	Average	1.2E+09	9.6E+08	10.0E+08	95.9	95.7	95.6	163.0	165.8	166.0	−0.11	−0.11	−0.11
RHC	0.2	6.4E+07	6.3E+07	5.9E+07	95.26	95.07	94.99	167.34	170.01	171.41	−0.11	−0.11	−0.11
	0.3	4.9E+07	4.94+07	4.7E+07	93.97	93.78	93.70	167.41	170.08	171.49	−0.11	−0.11	−0.11
	0.4	5.3E+06	5.7E+06	5.5E+06	82.51	82.32	82.24	168.07	170.77	172.19	−0.13	−0.13	−0.13
	0.5	4.2E+07	4.2E+07	4.0E+07	93.08	92.89	92.81	167.46	170.13	171.54	−0.11	−0.11	−0.11
	0.6	4.4E+07	4.3E+07	4.1E+07	93.29	93.09	93.01	167.44	170.12	171.53	−0.11	−0.11	−0.11
	0.7	1.0E+08	9.8E+07	9.2E+07	97.61	97.41	97.33	167.21	169.88	171.28	−0.11	−0.11	−0.11
	0.8	3.6E+08	3.4E+08	3.1E+08	104.22	104.02	103.94	166.87	169.53	170.93	−0.10	−0.10	−0.10
	Average	9.5E+07	9.1E+07	8.5E+07	94.28	94.08	94.00	167.40	170.07	171.48	−0.11	−0.11	−0.11
RHCM	0.2	6.7E+06	9.2E+06	1.1E+07	81.63	81.52	81.50	163.85	163.90	163.29	−0.13	−0.13	−0.13
	0.3	8.6E+08	1.1E+09	1.2E+09	106.07	105.96	105.94	162.54	162.56	161.94	−0.09	−0.09	−0.09
	0.4	1.1E+10	1.3E+10	1.5E+10	118.83	118.72	118.70	161.96	161.97	161.35	−0.07	−0.07	−0.07
	0.5	1.1E+10	1.2E+10	1.4E+10	118.77	118.66	118.64	161.97	161.97	161.36	−0.07	−0.07	−0.07
	0.6	5.3E+11	5.8E+11	6.6E+11	138.78	138.66	138.64	161.17	161.16	160.54	−0.04	−0.03	−0.03
	0.7	3.8E+12	4.0E+12	4.5E+12	148.81	148.70	148.68	160.82	160.80	160.18	−0.02	−0.02	−0.02
	0.8	6.6E+11	7.2E+11	8.2E+11	139.90	139.79	139.77	161.13	161.12	160.50	−0.03	−0.03	−0.03
	Average	7.1E+11	7.5E+11	8.5E+11	121.83	121.71	121.70	161.92	161.93	161.31	−0.06	−0.06	−0.06
RHC-starch	0.2	4.5E+03	5.2E+03	6.4E+03	43.26	43.02	43.01	158.32	163.10	162.24	−0.19	−0.19	−0.19
	0.3	7.2E+03	8.3E+03	1.0E+04	45.47	45.22	45.21	158.10	162.86	162.00	−0.19	−0.18	−0.18
	0.4	2.1E+04	2.3E+04	2.8E+04	50.40	50.16	50.15	157.63	162.37	161.51	−0.18	−0.18	−0.17
	0.5	7.1E+04	7.4E+04	9.0E+04	56.07	55.83	55.82	157.13	161.85	160.99	−0.17	−0.17	−0.16
	0.6	1.2E+06	1.1E+06	1.4E+06	69.47	69.23	69.22	156.13	160.80	159.94	−0.14	−0.14	−0.14
	0.7	2.5E+06	2.2E+06	2.7E+06	72.87	72.63	72.62	155.91	160.57	159.70	−0.14	−0.14	−0.14
	0.8	1.2E+07	9.9E+06	1.2E+07	80.24	80.00	79.99	155.45	160.09	159.22	−0.12	−0.13	−0.12
	Average	2.3E+06	1.9E+06	2.3E+06	59.69	59.44	59.43	156.95	161.66	160.80	−0.16	−0.16	−0.16

Table 5 (continued)

Sample	α	A/min^{-1}			ΔH/kJ mol^{-1}			ΔG/kJ mol^{-1}			ΔS/kJ mol^{-1} K^{-1}		
		20 °C min^{-1}	40 °C min^{-1}	50 °C min^{-1}	20 °C min^{-1}	40 °C min^{-1}	50 °C min^{-1}	20 °C min^{-1}	40 °C min^{-1}	50 °C min^{-1}	20 °C min^{-1}	40 °C min^{-1}	50 °C min^{-1}
RHCM-starch	0.2	1.7E+02	2.3E+02	2.2E+02	27.41	27.16	26.98	153.31	158.47	163.45	−0.22	−0.21	−0.21
	0.3	1.5E+03	1.8E+03	1.6E+03	36.70	36.45	36.26	152.08	157.18	162.11	−0.20	−0.20	−0.20
	0.4	6.6E+03	7.3E+03	6.2E+03	43.03	42.78	42.60	151.39	156.45	161.36	−0.19	−0.19	−0.19
	0.5	8.5E+03	9.3E+03	7.8E+03	44.17	43.92	43.74	151.28	156.33	161.24	−0.18	−0.18	−0.18
	0.6	1.2E+04	1.3E+04	1.1E+04	45.79	45.54	45.36	151.12	156.17	161.06	−0.18	−0.18	−0.18
	0.7	2.6E+04	2.7E+04	2.2E+04	49.09	48.84	48.66	150.81	155.85	160.73	−0.17	−0.17	−0.18
	0.8	1.8E+05	1.7E+05	1.3E+05	57.82	57.57	57.39	150.09	155.08	159.94	−0.16	−0.16	−0.16
	Average	3.4E+04	3.3E+04	2.6E+04	43.43	43.18	43.00	151.44	156.50	161.41	−0.19	−0.18	−0.19
RHCM-gelatin	0.2	9.5E+01	1.2E+02	1.5E+02	24.36	24.09	24.06	151.12	156.85	156.95	−0.22	−0.22	−0.22
	0.3	6.7E+03	7.1E+03	8.2E+03	42.36	42.09	42.06	148.82	154.42	154.51	−0.19	−0.19	−0.18
	0.4	2.7E+04	2.7E+04	3.1E+04	48.43	48.16	48.13	148.24	153.81	153.89	−0.17	−0.17	−0.17
	0.5	1.1E+05	1.1E+05	1.2E+05	54.73	54.47	54.43	147.71	153.25	153.32	−0.16	−0.16	−0.16
	0.6	1.6E+05	1.5E+05	1.7E+05	56.25	55.99	55.95	147.59	153.12	153.20	−0.16	−0.16	−0.16
	0.7	9.9E+05	8.3E+05	9.2E+05	64.37	64.11	64.07	146.99	152.49	152.56	−0.14	−0.15	−0.14
	0.8	2.8E+06	2.2E+06	2.5E+06	69.02	68.76	68.72	146.68	152.17	152.23	−0.14	−0.14	−0.14
	Average	5.8E+05	4.8E+05	5.3E+05	51.36	51.10	51.06	148.17	153.73	153.81	−0.17	−0.17	−0.17

94.0–94.3 kJ mol^{-1} and 121.7–121.8 kJ mol^{-1}, respectively. Similarly, average ΔH values for RHC-starch, RHCM-starch and RHCM-gelatin were 59.4–59.7 kJ mol^{-1}, 43.0–43.4 kJ mol^{-1}, and 51.1–51.4 kJ mol^{-1}, respectively.

Gibbs free energy reveals the overall energy change of the system, and lower ΔG values indicates favorable decomposition [52]. Average ΔG value ranges (depending on heating rate) of RH, RHC and RHCM were 163.0–166.0 kJ mol^{-1}, 167.4–171.5 kJ mol^{-1} and 161.3–161.9 kJ mol^{-1}, respectively. The high ΔG values obtained in this study indicated that thermal decomposition of RH, RHC and RHCM is a non-spontaneous process [96]. The values of Gibbs free energy were found in the same range when compared to values by other authors for rice husks (165.0 kJ mol^{-1}) [94] and rice bran (167.2 kJ mol^{-1}) [97]. In fact, the average ΔG values for developed RHC-starch, RHCM-starch and RHCM-gelatin were 157.0–161.7 kJ mol^{-1}, 151.4–161.4 kJ mol^{-1}, and 148.2–153.8 kJ mol^{-1}, respectively.

The change in entropy (ΔS) is a measure of disorders, and a negative ΔS value depicts decreased disorders of the system, i.e., ordered product formation [52]. The low and negative value obtained for RH, RHC, RHCM and RH-biocomposites revealed that extended time is required for thermal decomposition of active material in the rice husks [30, 54, 98]. This characteristic makes rice husks an attractive component for biocomposites because for their application, and thermal decomposition is typically less desirable. Low and negative values were upheld, no matter the heating rate utilized, meaning that heating rate had no striking effect on the entropy change of the RH, RHC, RHCM and RH-biocomposites.

Conclusions

Pyrolysis of RH, RHC, RCM and three RH-biocomposites by thermogravimetric analysis (TGA) was carried out to determine combustion and kinetic parameters at three different heating rates of 20, 40 and 50 °C min^{-1}. As expected, the TGA established that with an increase in heating rates, the degradation curves moved toward upper-temperature regions, signaling enhanced decomposition temperature due to shorter exposure time. Maximum combustion rates were around 0.57–0.59% min^{-1}, 1.03% min^{-1} and 0.63–0.69% min^{-1} for RH, RHC and RHCM, respectively. The maximum combustion rates of RH-biocomposites were in a 0.76–0.97% min^{-1} range. Lower values for combustion rate signify enhanced flame retardancy. Average pre-exponential factors using KAS method for RH, RHC and RHCM were in the 0.24E + 00–1.10E + 03 range, respectively, while those for OFW method were in the 1.57E + 08–7.04E + 11 range, respectively. For developed RH-biocomposites, average pre-exponential factors using KAS method were in the 2.24E-03–8.07E-03 range, respectively, while those for OFW method were in the 7.75E + 04–4.55E + 06 range, respectively. Average activation energy of RH, RHC and RHCM was 95.9 kJ mol^{-1}, 94.0 kJ mol^{-1} and 123.4 kJ mol^{-1}, respectively, using the KAS method. The respective activation energies using the OFW method were 101.2 kJ mol^{-1}, 99.7 kJ mol^{-1} and 127.1 kJ mol^{-1}. For RHC-starch, RHCM-starch and RHCM-gelatin biocomposites, activation energies were 58.2 kJ mol^{-1}, 41.0 kJ mol^{-1} and 49.5 kJ mol^{-1} as well as 67.7 kJ mol^{-1}, 48.3 kJ mol^{-1} and 56.1 kJ mol^{-1} for KAS and OFW methods, respectively. Average ΔG value ranges (depending on heating rate) of RH, RHC and RHCM were 163.0–166.0 kJ mol^{-1}, 167.4–171.5 kJ mol^{-1} and 161.3–161.9 kJ mol^{-1}, respectively. The average ΔG values for developed RHC-starch, RHCM-starch and RHCM-gelatin biocomposites were 157.0–161.7 kJ mol^{-1}, 151.4–161.4 kJ mol^{-1}, and 148.2–153.8 kJ mol^{-1}, respectively. There was a clear relation between the conversion degree and activation energy, which indicated complexity of the rice husks combustion process. The low-energy barrier ($\leq$ 5.4 kJ mol^{-1}) between the activation energies and ΔH values for the process indicated that reaction initiation occurs easily. Generally, the obtained results from this study can guide the application of rice husk-derived materials to suitable fields as well as to suitable disposal methods.

Acknowledgements This work was supported by the Swedish Research Council (VR) under the Swedish Research Links Network Grant for International collaboration (grant no. 2020-03725) entitled "Bioplastic development from agricultural residues in Uganda". Technical support from Yosevi Engineering Services Limited, www.yosevi.com as well as Mr. Edward Mukasa from the Department of chemistry, Makerere University is gratefully acknowledged.

Author contributions Conceptualization was done by VAY, ML and MH. The experimental design and experimentation were done by VAY and MK. The methodology was done by VAY, MK and ML. All authors contributed to writing the manuscript as well as reviewing and editing it. KHA and EK were involved in investigations. Supervision and funds acquisition were done by ML, MH and KHA.

Funding Open access funding provided by Royal Institute of Technology. This work was supported by the Swedish Research Council (VR) under the Swedish Research Links Network Grant for International collaboration (grant no. 2020–03725) entitled "Bioplastic development from agricultural residues in Uganda".

Data availability The datasets generated during and/or analyzed during the current study are available from the corresponding author on reasonable request.

Declarations

Conflict of interest The authors have no relevant financial or non-financial interests to disclose.

References

1. Nsubuga D, Banadda N, Kiggundu N. Innovations in value-addition of agricultural by-products in Uganda. J Environ Protect. 2019;10:1493–506.
2. Menya E, Olupot PW, Storz H, Lubwama M, Kiros Y. Characterization and alkaline pretreatment of rice husk varieties in Uganda for potential utilization as precursors in the production of activated carbon and other value-added products. Waste Manag. 2018;81:104–16.
3. Lubwama M, Yiga VA. Characteristics of briquettes developed from rice and coffee husks for domestic cooking applications in Uganda. Renew Energy. 2018;118:43–55.
4. Food and Agriculture Organization (FAO), Food and Agriculture Policy Design Analysis-Uganda, Country Fact Sheet on Food and Agriculture Policy trends. 2015.
5. Bariani M, Boix E, Cassella F, Cabrera MN. Furfural production from rice husks within a biorefinery framework. Biomass Convers Biorefin. 2021;11(3):781–94.
6. Norhasnan NHA, Hassan MZ, Nor AFM, Zaki SA, Dolah R, Jamaludin KR, Aziz SAA. Physicomechanical properties of rice husk/coco peat reinforced acrylonitrile butadiene styrene blend composites. Polymers. 2021;13(7):1171.
7. Musinguzi TL, Yiga VA, Lubwama M. Production of bio-composite polymers with rice and coffee husks as reinforcing fillers using a low-cost compression molding machine. J Eng Agric Environ. 2019;5(1):61–72.
8. Yiga VA, Pagel S, Lubwama M, Epple S, Olupot PW, Bonten C. Development of fiber-reinforced polypropylene with NaOH pretreated rice and coffee husks as fillers: mechanical and thermal properties. J Thermoplast Compos Mater. 2020;33(9):1269–91.
9. Alvarez J, Lopez G, Amutio M, Bilbao J, Olazar M. Upgrading the rice husk char obtained by flash pyrolysis for the production of amorphous silica and high quality activated carbon. Biores Technol. 2014;170:132–7.
10. Rabe S, Sanchez-Olivares G, Pérez-Chávez R, Schartel B. Natural keratin and coconut fibres from industrial wastes in flame retarded thermoplastic starch biocomposites. Materials. 2019;12(3):344.
11. Monte LS, Escócio VA, de Sousa AMF, Furtado CRG, Leite MCAM, Visconte LLY, Pacheco EBAV. Study of time reaction on alkaline pretreatment applied to rice husk on biomass component extraction. Biomass Convers Biorefin. 2018;8(1):189–97.
12. Tsang YF, Kumar V, Samadar P, Yang Y, Lee J, Ok YS, Song H, Kim KH, Kwon EE, Jeon YJ. Production of bioplastic through food waste valorization. Environ Int. 2019;127:625–44.
13. Ahimbisibwe M, Banadda N, Seay J, Nabuuma B, Atwijukire E, Wembabazi E, Nuwamanya E. Influence of weather and purity of plasticizer on degradation of cassava starch bioplastics in natural environmental conditions. J Agric Chem Environ. 2019;8(04):237.
14. Vyazovkin S, Burnham AK, Criado JM, Pérez-Maqueda LA, Popescu C, Sbirrazzuoli N. ICTAC Kinetics Committee recommendations for performing kinetic computations on thermal analysis data. Thermochim Acta. 2011;520(1–2):1–19.
15. Yiga VA, Lubwama M, Olupot PW. Pyrolysis, kinetics and thermodynamic analyses of rice husks/clay fiber-reinforced polylactic acid composites using thermogravimetric analysis. J Therm Anal Calorim. 2023; 148: 3457–3477. https://doi.org/10.1007/s10973-022-11927-y
16. Kasmiarno LD, Steven S, Rizkiana J, Restiawaty E, Bindar Y. Kinetic studies and performance analysis of Indonesian rice husk pyrolysis. In: IOP Conference Series: Materials Science and Engineering (Vol. 1143, No. 1, p. 012067). IOP Publishing, 2021.
17. Chandrasekaran A, Ramachandran S, Subbiah S. Determination of kinetic parameters in the pyrolysis operation and thermal behavior of *Prosopis juliflora* using thermogravimetric analysis. Biores Technol. 2017;233:413–22.
18. El-Sayed SA, Mostafa ME. Kinetic parameters determination of biomass pyrolysis fuels using TGA and DTA techniques. Waste Biomass Valoriz. 2015;6(3):401–15.
19. Ma Z, Chen D, Gu J, Bao B, Zhang Q. Determination of pyrolysis characteristics and kinetics of palm kernel shell using TGA–FTIR and model-free integral methods. Energy Convers Manag. 2015;89:251–9.
20. Liu J, Jiang X, Cai H, Gao F. Study of combustion characteristics and kinetics of agriculture briquette using thermogravimetric analysis. ACS Omega. 2021;6:15827–33.
21. Jia C, Chen J, Liang J, Song S, Liu K, Jiang A, Wang Q. Pyrolysis characteristics and kinetic analysis of rice husk. J Therm Anal Calorim. 2020;139(1):577–87.
22. Kumar M, Mishra PK, Upadhyay SN. Thermal degradation of rice husk: effect of pre-treatment on kinetic and thermodynamic parameters. Fuel. 2020;268: 117164.
23. Singh P, Singh RK, Gokul PV, Hasan SU, Sawarkar AN. Thermal degradation and pyrolysis kinetics of two Indian rice husk varieties using thermogravimetric analysis. Energy Sour Part A Recovery Util Environ Eff. 2020. https://doi.org/10.1080/15567036.2020.1736215.
24. Yuan R, Yu S, Shen Y. Pyrolysis and combustion kinetics of lignocellulosic biomass pellets with calcium-rich wastes from agroforestry residues. Waste Manag. 2019;87:86–96.
25. Lim ACR, Chin BLF, Jawad ZA, Hii KL. Kinetic analysis of rice husk pyrolysis using Kissinger-Akahira-Sunose (KAS) method. Proced Eng. 2016;148:1247–51.
26. Rasool T, Srivastava VC, Khan MNS. Bioenergy potential of *Salix alba* assessed through kinetics and thermodynamic analyses. Process Integr Optim Sustain. 2018;2(3):259–68.
27. Gajera ZR, Verma K, Tekade SP, Sawarkar AN. Kinetics of co-gasification of rice husk biomass and high sulphur petroleum coke with oxygen as gasifying medium via TGA. Bioresour Technol Rep. 2020;100479:1–10.
28. Wang T, Fu T, Chen K, Cheng R, Chen S, Liu J, Mei M, Li J, Xue Y. Co-combustion behavior of dyeing sludge and rice husk by using TG–MS: thermal conversion, gas evolution, and kinetic analyses. Bioresour Technol. 2020;311:123527.
29. El-Sayed S. Thermal decomposition, kinetics and combustion parameters determination for two different sizes of rice husk using TGA. Eng Agric Environ Food. 2019;12(4):460–9.
30. Loy ACM, Gan DKW, Yusup S, Chin BLF, Lam MK, Shahbaz M, Unrean P, Acda MN, Rianawati E. Thermogravimetric kinetic modelling of in-situ catalytic pyrolytic conversion of rice husk to bioenergy using rice hull ash catalyst. Bioresour Technol. 2018;261:213–22.
31. Zhang S, Dong Q, Zhang L, Xiong Y. Effects of water washing and torrefaction on the pyrolysis behavior and kinetics of rice husk through TGA and Py-GC/MS. Biores Technol. 2016;199:352–61.

32. Gu S, Zhou J, Luo Z, Wang Q, Shi Z. Kinetic study on the preparation of silica from rice husk under various pretreatments. J Therm Anal Calorim. 2015;119(3):2159–69.
33. Muazu RI, Stegemann JA. Effects of operating variables on durability of fuel briquettes from rice husks and corn cobs. Fuel Process Technol. 2015;133:137–45.
34. Yoon PR, Choi JY. Effects of shift in growing season due to climate change on rice yield and crop water requirements. Paddy Water Environ. 2020;18(2):291–307.
35. Gupta H, Kumar H, Gehlaut AK, Singh SK, Gaur A, Sachan S, Park JW. Preparation and characterization of bio-composite films obtained from coconut coir and groundnut shell for food packaging. J Mater Cycles Waste Manag. 2022;24(2):569–81.
36. Gupta H, Kumar H, Kumar M, Gehlaut AK, Gaur A, Sachan S, Park JW. Synthesis of biodegradable films obtained from rice husk and sugarcane bagasse to be used as food packaging material. Environ Eng Res. 2020;25(4):506–14.
37. Abdul Rahman NH, Chieng BW, Ibrahim NA, Abdul Rahman N. Extraction and characterization of cellulose nanocrystals from tea leaf waste fibers. Polymers. 2017;9(11):588.
38. Orhan B, Ziba CA, Morcali MH, Dolaz M. Synthesis of hydroxyethyl cellulose from industrial waste using microwave irradiation. Sustain Environ Res. 2018;28(6):403–11.
39. Holik HA, Sianne M, Rahayu D. Cellulose from elephant grass leaves (*Pennisetum purpureum* Schumach.) as an alternative of bioplastic material. World J Pharm Sci. 2014; 436–442.
40. Moran JI, Vazquez A, Cyras VP. Bio-nanocomposites based on derivatized potato starch and cellulose, preparation and characterization. J Mater Sci. 2013;48(20):7196–203.
41. Hamin SH, Sayid Abdullah SHY, Lananan F, Abdul Hamid SH, Kasan NA, Mohamed NN, Endut A. Effect of chemical treatment on the structural, thermal, and mechanical properties of sugarcane bagasse as filler for starch-based bioplastic. J Chem Technol Biotechnol. 2023;98(3):625–632.
42. Lubwama M, Yiga VA. Development of groundnut shells and bagasse briquettes as sustainable fuel sources for domestic cooking applications in Uganda. Renew Energy. 2017;111:532–42.
43. Sahoo D, Remya N. Influence of operating parameters on the microwave pyrolysis of rice husk: biochar yield, energy yield, and property of biochar. Biomass Convers Biorefin. 2020;12:3447–56.
44. Liu H, J E, Ma X, Xie C. Influence of microwave drying on the combustion characteristics of food waste. Dry Technol. 2016;34(12):1397–405.
45. Song A, Zha F, Tang X, Chang Y. Effect of the additives on combustion characteristics and desulfurization performance of cow dung briquette. Chem Eng Process Process Intensif. 2019;143: 107585.
46. Xiao R, Yang W, Cong X, Dong K, Xu J, Wang D, Yang X. Thermogravimetric analysis and reaction kinetics of lignocellulosic biomass pyrolysis. Energy. 2020;201: 117537.
47. Das P, Tiwari P. Thermal degradation kinetics of plastics and model selection. Thermochim Acta. 2017;654:191–202.
48. Akahira T, Sunose TT. Trans. Joint convention of four electrical institutes. Res Rep Chiba Inst Technol. 1971;16:22–31.
49. Doyle CD. Series approximations to the equation of thermogravimetric data. Nature. 1965;207(4994):290–1.
50. Ozawa T. A new method of analyzing thermogravimetric data. Bull Chem Soc Jpn. 1965;38(11):1881–6.
51. Mishra RK, Mohanty K. Kinetic analysis and pyrolysis behaviour of waste biomass towards its bioenergy potential. Biores Technol. 2020;311: 123480.
52. Pindar S, Dhawan N. Kinetics and thermodynamical evaluation of electrode material of discarded lithium-ion batteries and its impact on recycling. J Therm Anal Calorim. 2021;146(4):1819–31.
53. Singh G, Varma AK, Almas S, Jana A, Mondal P, Seay J. Pyrolysis kinetic study of waste milk packets using thermogravimetric analysis and product characterization. J Mater Cycles Waste Manag. 2019;21(6):1350–60.
54. Mehmood MA, Ye G, Luo H, Liu C, Malik S, Afzal I, Xu J, Ahmad MS. Pyrolysis and kinetic analyses of Camel grass (*Cymbopogon schoenanthus*) for bioenergy. Bioresour Technol. 2017;228:18–24.
55. Yiga VA, Lubwama M, Olupot PW. Thermal stability of unmodified and alkali-modified rice husks for flame retardant fiber-reinforced PLA composites. J Therm Anal Calorim. 2022;147(20):11049–75.
56. Dhaneswara D, Fatriansyah JF, Wardana AK, Haqoh AN, Khairunnisa SA. The Study of thermal decomposition of rice husk in silica production: the effect of hydrochloric acid leaching. In: IOP Conference Series: Materials Science and Engineering (Vol. 547, No. 1, p. 012032). IOP Publishing. 2019.
57. Wang X, Lu Z, Jia L, Chen J. Physical properties and pyrolysis characteristics of rice husks in different atmosphere. Results Phys. 2016;6:866–8.
58. Wang Z, Yao Z, Zhou J, Zhang Y. Reuse of waste cotton cloth for the extraction of cellulose nanocrystals. Carbohyd Polym. 2017;157:945–52.
59. Garcia D, López J, Balart R, Ruseckaite RA, Stefani PM. Composites based on sintering rice husk–waste tire rubber mixtures. Mater Des. 2007;28(7):2234–8.
60. Ludueña L, Fasce D, Alvarez VA, Stefani PM. Nanocellulose from rice husk following alkaline treatment to remove silica. BioResources. 2011;6(2):1440–53.
61. Wu S, Zhang J, Li C, Wang F, Shi L, Tao M, Weng B, Yan B, Guo Y, Chen Y. Characterization of potential cellulose fiber from cattail fiber: a study on micro/nano structure and other properties. Int J Biol Macromol. 2021;193:27–37.
62. Abraham E, Deepa B, Pothan LA, Jacob M, Thomas S, Cvelbar U, Anandjiwala R. Extraction of nanocellulose fibrils from lignocellulosic fibres: a novel approach. Carbohyd Polym. 2011;86(4):1468–75.
63. Rashid S, Dutta H. Characterization of nanocellulose extracted from short, medium and long grain rice husks. Ind Crops Prod. 2020;154: 112627.
64. Ab Ghani MH, Royan NRR, Kang SW, Sulong AB, Ahmad S. Effect of alkaline treated rice husk on the mechanical and morphological properties of recycled HDPE/RH Composite. J Appl Sci Agric. 2015;10(5):138–44.
65. Johar N, Ahmad I. Morphological, thermal, and mechanical properties of starch biocomposite films reinforced by cellulose nanocrystals from rice husks. BioResources. 2012;7(4):5469–77.
66. Nascimento P, Marim R, Carvalho G, Mali S. Nanocellulose produced from rice hulls and its effect on the properties of biodegradable starch films. Mater Res. 2016;19:167–74.
67. Yap SY, Sreekantan S, Hassan M, Sudesh K, Ong MT. Characterization and biodegradability of rice husk-filled polymer composites. Polymers. 2020;13(1):104.
68. Bisht N, Gope PC, Rani N. Rice husk as a fibre in composites: a review. J Mech Behav Mater. 2020;29(1):147–62.
69. Montero B, Rico M, Barral L, Bouza R, López J, Schmidt A, Bittmann-Hennes B. Preparation and characterization of bionanocomposite films based on wheat starch and reinforced with cellulose nanocrystals. Cellulose. 2021;28(12):7781–93.
70. Huang D, Zheng Y, Quan Q. Enhanced mechanical properties and UV shield of carboxymethyl cellulose films with polydopamine-modified natural fibre-like palygorskite. Appl Clay Sci. 2019;183: 105314.
71. Marichelvam MK, Jawaid M, Asim M. Corn and rice starch-based bio-plastics as alternative packaging materials. Fibers. 2019;7(4):32.

72. Onoja DA, Ahemen I, Iorfa TF. Synthesis and characterization of cellulose based nanofibres from rice husk. J Appl Phys. 2019;11:80–7.
73. Mohammed IY, Lim CH, Kazi FK, Yusup S, Lam HL, Abakr YA. Co-pyrolysis of rice husk with underutilized biomass species: a sustainable route for production of precursors for fuels and valuable chemicals. Waste Biomass Valoriz. 2017;8(3):911–21.
74. Amin MR, Chowdhury MA, Kowser MA. Characterization and performance analysis of composite bioplastics synthesized using titanium dioxide nanoparticles with corn starch. Heliyon. 2019;5(8): e02009.
75. Nanda S, Dalai AK, Berruti F, Kozinski JA. Biochar as an exceptional bioresource for energy, agronomy, carbon sequestration, activated carbon and specialty materials. Waste Biomass Valoriz. 2016;7(2):201–35.
76. Flores JJA, Quiñones JGR, Rodríguez MLÁ, Vera JVA, Valencia JE, Martínez SJG, Montesino FM, Rosas AA. Thermal degradation kinetics and FT-IR analysis on the pyrolysis of *Pinus pseudostrobus*, *Pinus leiophylla* and *Pinus montezumae* as forest waste in Western Mexico. Biomass Energy Appl. 2020;153–177.
77. Mishra RK, Mohanty K. Pyrolysis kinetics and thermal behavior of waste sawdust biomass using thermogravimetric analysis. Biores Technol. 2018;251:63–74.
78. Krishnamurthy A, Amritkumar P. Synthesis and characterization of eco-friendly bioplastic from low-cost plant resources. SN Appl Sci. 2019;1(11):1–13.
79. Adebisi JA, Agunsoye JO, Bello SA, Kolawole FO, Ramakokovhu MM, Daramola MO, Hassan SB. Extraction of silica from sugarcane bagasse, cassava periderm and maize stalk: proximate analysis and physico-chemical properties of wastes. Waste Biomass Valoriz. 2019;10(3):617–29.
80. Sánchez-Safont EL, Aldureid A, Lagarón JM, Gamez-Perez J, Cabedo L. Effect of the purification treatment on the valorization of natural cellulosic residues as fillers in PHB-based composites for short shelf life applications. Waste Biomass Valoriz. 2021;12(5):2541–56.
81. Tan SX, Ong HC, Andriyana A, Lim S, Pang YL, Kusumo F, Ngoh GC. Characterization and parametric study on mechanical properties enhancement in biodegradable chitosan-reinforced starch-based bioplastic film. Polymers. 2022;14(2):278.
82. Gonzalez-Arias J, Fernandez C, Rosas JG, Bernal MP, Clemente R, Sanchez ME, Gomez X. Integrating anaerobic digestion of pig slurry and thermal valorisation of biomass. Waste Biomass Valoriz. 2020;11(11):6125–37.
83. Singha S, Mahmutovic M, Zamalloa C, Stragier L, Verstraete W, Svagan AJ, Das O, Hedenqvist MS. Novel bioplastic from single cell protein as a potential packaging material. ACS Sustain Chem Eng. 2021;9(18):6337–46.
84. Awad AH, Abdel-Ghany AW, El-Wahab A, Ayman A, El-Gamasy R, Abdellatif MH. The influence of adding marble and granite dust on the mechanical and physical properties of PP composites. J Therm Anal Calorim. 2020;140(6):2615–23.
85. Carosio F, Fina A. Three organic/inorganic nanolayers on flexible foam allow retaining superior flame retardancy performance upon mechanical compression cycles. Front Mater. 2019;6:20.
86. Cai Z, Ma X, Fang S, Yu Z, Lin Y. Thermogravimetric analysis of the co-combustion of eucalyptus residues and paper mill sludge. Appl Therm Eng. 2016;106:938–43.
87. Kavitha D, Murugavel SC, Thenmozhi S. Flame retarding cardanol based novolac-epoxy/rice husk composites. Mater Chem Phys. 2021;263: 124225.
88. Loganathan TM, Sultan MTH, Ahsan Q, Jawaid M, Naveen J, Shah AUM, Hua LS. Characterization of alkali treated new cellulosic fibre from *Cyrtostachys renda*. J Market Res. 2020;9(3):3537–46.
89. Damartzis T, Vamvuka D, Sfakiotakis S, Zabaniotou A. Thermal degradation studies and kinetic modeling of cardoon (*Cynara cardunculus*) pyrolysis using thermogravimetric analysis (TGA). Biores Technol. 2011;102(10):6230–8.
90. Goenka R, Parthasarathy P, Gupta NK, Biyahut NK, Narayanan S. Kinetic analysis of biomass and comparison of its chemical compositions by thermogravimetry, wet and experimental furnace methods. Waste Biomass Valoriz. 2015;6(6):989–1002.
91. Yuan G, Liang R, Duan E, Liu R. Co-combustion characteristics and kinetic analysis of three different wastes of antibiotic fermentation and coal. Sustain Energy Fuels. 2023;7(8):1793–803.
92. Bhattacharjee N, Biswas AB. Physicochemical analysis and kinetic study of orange bagasse at higher heating rates. Fuel. 2020;271: 117642.
93. Ceylan S, Topçu Y. Pyrolysis kinetics of hazelnut husk using thermogravimetric analysis. Biores Technol. 2014;156:182–8.
94. Rasool T, Srivastava VC, Khan MNS. Kinetic and thermodynamic analysis of thermal decomposition of deodar (*Cedrus deodara*) saw dust and rice husk as potential feedstock for pyrolysis. Int J Chem React Eng. 2019; 17(1). pp. 20170184. https://doi.org/10.1515/ijcre-2017-0184
95. Asim M, Paridah MT, Chandrasekar M, Shahroze RM, Jawaid M, Nasir M, Siakeng R. Thermal stability of natural fibers and their polymer composites. Iran Polym J. 2020;29(7):625–48.
96. Naqvi SR, Tariq R, Hameed Z, Ali I, Taqvi SA, Naqvi M, Niazi MB, Noor T, Farooq W. Pyrolysis of high-ash sewage sludge: thermo-kinetic study using TGA and artificial neural networks. Fuel. 2018;233:529–38.
97. Xu Y, Chen B. Investigation of thermodynamic parameters in the pyrolysis conversion of biomass and manure to biochars using thermogravimetric analysis. Biores Technol. 2013;146:485–93.
98. Singh RK, Ruj B. Time and temperature depended fuel gas generation from pyrolysis of real world municipal plastic waste. Fuel. 2016;174:164–71.